

Volatile Organic Compound Detection Using Insect Odorant-Receptor Functionalised Field-Effect Transistors

by

Eddyn Oswald Perkins Treacher

A thesis submitted in fulfilment of the
requirements of the degree of
Doctor of Philosophy in Physics
School of Physical and Chemical Sciences
Te Herenga Waka - Victoria University of Wellington

Nov 2023



Table of contents

Acknowledgements	1
1. Verifying Non-Covalent Functionalisation of Carbon Nanotubes and Graphene	3
1.1. Non-Covalent Bonding and π -Stacking	3
1.2. Attachment of 1-Pyrenebutanoic Acid N-Hydroxysuccinimide Ester	5
1.2.1. Comparing Attachment Methods	5
1.2.2. Examining 1-Pyrenebutanoic Acid N-Hydroxysuccinimide Ester Purity	9
1.2.3. Electrical Characterisation	9
1.3. Attachment of 1-Pyrenebutyric Acid	13
1.3.1. Comparing Attachment Methods	13
1.3.2. Raman Spectroscopy	13
1.3.3. Electrical Characterisation	15
1.4. Attachment of PEGlyated Pyrene-Based Linkers	16
1.4.1. Pyrene-NTA, Pyrene-Biotin and PEGylation	16
1.4.2. Fluorescence Characterisation with Pyrene-PEG-FITC	17
1.4.3. Electrical Characterisation with Pyrene-PEG	19
1.5. Verifying Linker-Receptor Attachment	20
1.5.1. Functionalisation with GFP-OR Nanodiscs using PBASE	20
1.5.2. Functionalisation with GFP-OR Nanodiscs using Pyrene-PEG-NTA	22
1.6. Overcoming Issues with Functionalisation	24
1.6.1. Hydrophobicity of Carbon Nanotubes and Graphene	24
1.6.2. Photoresist Contamination	25
1.6.3. Interactions between Substrate and Pyrene(-PEG)	27
1.6.4. “Coffee-Ring” Effect	27
1.7. Conclusions	29
Appendices	31
A. Python Code for Data Analysis	31
A.1. Code Repository	31
A.2. Atomic Force Microscope Histogram Analysis	31
A.3. Raman Spectroscopy Analysis	32
A.4. Field-Effect Transistor Analysis	32

Table of contents

B. Vapour Delivery System	35
B.1. Technical Notes	35
B.2. Future Improvements	35

Acknowledgements

69450

Rifat, Alex - vapour sensor
Erica Cassie - FET sensing setup
Rob Keyzers and Jennie Ramirez-Garcia - NMR spectra
Patricia Hunt - Computational chemistry

1. Verifying Non-Covalent Functionalisation of Carbon Nanotubes and Graphene

272688

In previous chapters, we have discussed methods of fabricating carbon nanotube and graphene devices and then shown that they can be operated effectively as chemical sensors. However, to detect specific chemical traces while ignoring others ('specific sensing'), the devices require chemical modification, often called 'functionalisation'. Instead of responding to stimuli themselves, the sensing signal is picked up by attached receptors. The devices then act as passive transducers for the received signal. Receptors previously used with carbon nanotube and graphene devices include aptamers and a range of proteins, including odorant receptors. A common approach to attaching receptors to the transducer involves the use of a linker molecule to tether the receptor to the transducer. Verifying that this linker molecule is bridging between the transducer and the receptor element is important for a complete understanding of the behaviour of these sensors. This verification involves providing evidence for effective attachment of linker molecule to the transducing device channel, then showing successful tethering of odorant receptors and other biomolecules to the attached linker molecule.

This chapter therefore takes some time to explore the attachment of linker molecules to carbon nanotube and graphene device channels. The linker molecules used are discussed in detail, and numerous hurdles to successful functionalisation via linker molecules are identified and addressed. Next, it looks at verifying that the odorant receptor proteins of interest have specifically attached to these linker molecules. The experimental parameters used for both the attachment of linker molecules and receptor proteins are also varied, and the impact of these variations on successful functionalisation is investigated. Verification methods used in this chapter include Raman spectroscopy, fluorescence microscopy and electrical characterisation.

1.1. Non-Covalent Bonding and π -Stacking

Linker molecules may be attached via covalent or non-covalent bonding to carbon nano-materials, such as carbon nanotubes and graphene. Covalent bonding is stronger than

1. Verifying Non-Covalent Functionalisation of Carbon Nanotubes and Graphene

non-covalent bonding, and therefore gives a more permanent attachment between linker molecules and the transducer. However, non-covalent bonding has the advantage of having less of an impact on the structure of a nanomaterial than covalent bonding, meaning non-covalent bonding is less likely to negatively affect the electrical properties of the transducer [1]–[4]. For example, one group found covalent bonding of diazonium linker caused a $\sim 50\%$ drop in graphene channel mobility [5]. In comparison, only a $\sim 5\%$ drop in mobility was seen for attachment of a mixture of linkers containing pyrene to a graphene channel via non-covalent π stacking [6].

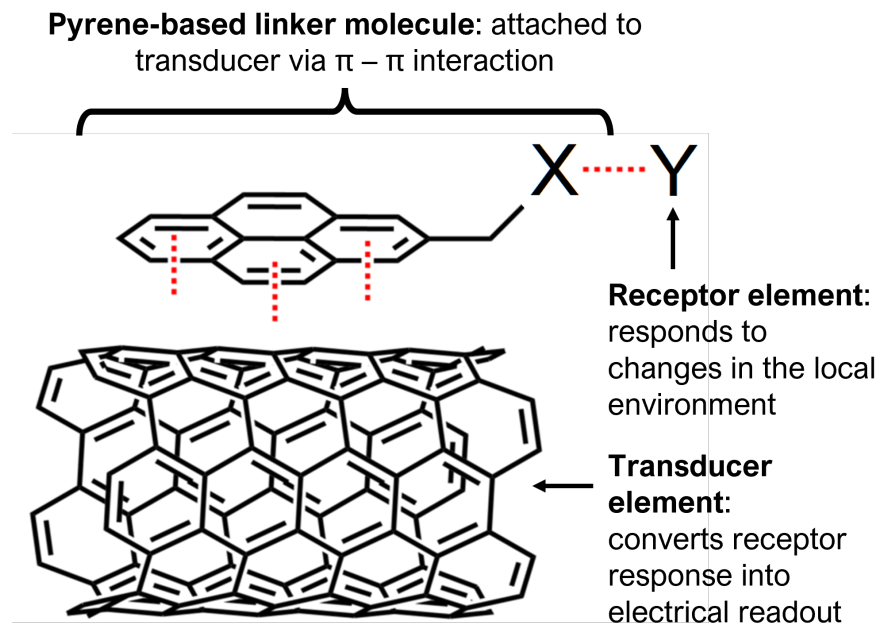


Figure 1.1.: Attachment of pyrene-based linker molecule pyrene-X and receptor Y to a carbon nanotube, representing the transducer element of a field-effect transistor. Source: Adapted from [7].

π -stacking or $\pi - \pi$ interaction is often used to describe a type of non-covalent bonding which occurs due to dispersion forces between unsaturated polycyclic molecules [8]. It has been argued that this label is unhelpfully specific and a misrepresentation of what can be simply classed as a type of Van Der Waals bonding [8], [9]. However, as the use of the term is widespread in the literature, it is also used here for ease of reference. Carbon nanotubes and graphene consist of a network of carbon atoms attached to each other by sp^2 hybrid orbitals in a polycyclic structure. They are therefore able to strongly interact with linker molecules with aromatic moieties, such as pyrene [4], [8], [10]. Figure 1.1 is a visual demonstration of the relationship between the pyrene-based linker molecule with the transducer and receptor elements. A wide range of pyrene-based linker molecules have been used for non-covalent modification of carbon nanotubes and graphene [11]. π -stacking with pyrene is the bonding mechanism underlying all the functionalisation

1.2. Attachment of 1-Pyrenebutanoic Acid N-Hydroxysuccinimide Ester

processes in this thesis.

1.2. Attachment of 1-Pyrenebutanoic Acid N-Hydroxysuccinimide Ester

1.2.1. Comparing Attachment Methods

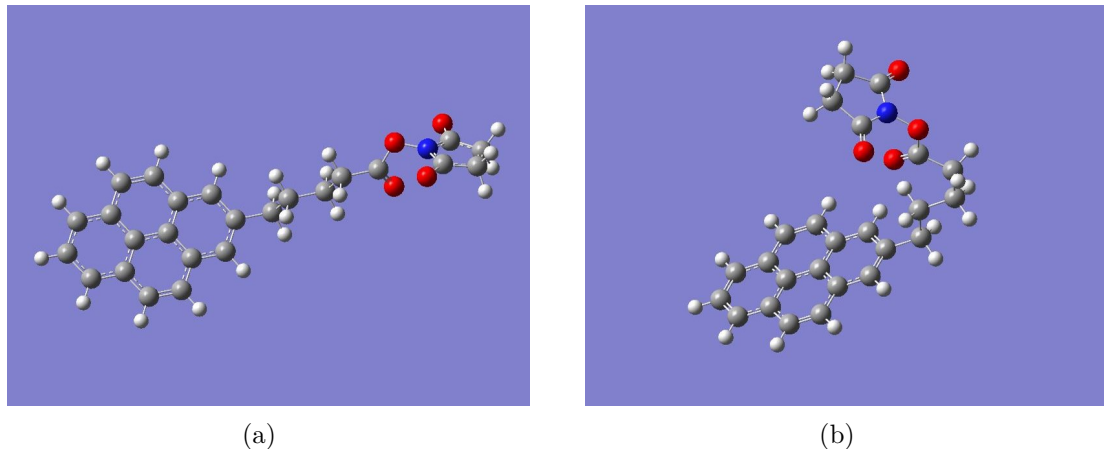


Figure 1.2.: Two conformations of PBASE molecule with geometry optimised via *ab initio* calculations (computed using Gaussian 16 [12]). White balls correspond to hydrogen, grey to carbon, red to oxygen and blue to nitrogen. The conformation in (a) has a Hartree-Fock energy of -3427728.67 kJ/mol, while the conformation in (b) has a Hartree-Fock energy of -3427729.66 kJ/mol. The difference between computed Hartree-Fock energies is 1.0 kJ/mol, small enough that the existence of both molecular conformations is physically feasible.

1-Pyrenebutanoic acid N-hydroxysuccinimide ester (variously known commercially and in the literature as 1-Pyrenebutyric acid N-hydroxysuccinimide ester, PBASE, PBSE, PASE, Pyr-NHS, PyBASE, PANHS) is a aromatic molecule commonly used for tethering biomolecules to the carbon rings of graphene and carbon nanotubes. The molecular structure of PBASE is shown in Figure 1.2. Two locally stable molecular conformations were found to exist, a straight (Figure 1.2a) and bent (Figure 1.2b) structure. Similar locally stable structures have previously been computed for PBASE attached to graphene [13]. The pyrene moiety, seen on the left-hand side of Figure 1.2, non-covalently bonds to the carbon rings of the carbon nanotube and graphene surface. The N-hydroxysuccinimide (NHS) ester group, seen on the right-hand side of Figure 1.2, is highly reactive with amine groups. It can undergo a nucleophilic substitution reaction with amines attached to proteins or aptamers, tethering these biomolecules via an amide or imide bond [4], [10], [14], [15].

1. Verifying Non-Covalent Functionalisation of Carbon Nanotubes and Graphene

Table 1.1.: Comparison of PBASE functionalisation processes used for immobilisation of proteins and aptamers onto carbon nanotubes and graphene. Experimentally optimised variables are marked with a star (*). Blank entries indicate there was no mention of the parameter in a particular paper.

Solvent	Channel	Conc. (mM)	Incubation type	Time (hr)	Rinse steps	References
DMF	CNT	5	Immersed	1	PBS	Maehashi <i>et al.</i> [16]
		6	Immersed	1	DMF, PBS	García-Aljaro <i>et al.</i> [17]
		6	Immersed	1	DMF	Chen <i>et al.</i> [14]
		6	Immersed	1	DMF	Cella <i>et al.</i> [18]
		6	Immersed	1	DMF	Das <i>et al.</i> [19]
		6	-	2	DMF	Besteman <i>et al.</i> [20]
	Graphene	-	-	2	DMF	Kwong Hong Tsang <i>et al.</i> [21]
		-	-	20	-	Wiedman <i>et al.</i> [22]
		0.2	Immersed	20	DMF, IPA, DI water	Gao <i>et al.</i> [23]
		1	100 μ L droplet	6	DMF, IPA, DI water	Nekrasov <i>et al.</i> [24]
		5	Immersed	1	DMF, DI water	Hwang <i>et al.</i> [25]
		5*	Immersed	3*	DMF	Hao <i>et al.</i> [26]
		5	Immersed, with agitation	4*	DMF, DI water	Mishyn <i>et al.</i> [4]
		6	6 μ L droplet	2	DMF, DI water	Nur Nasufiya <i>et al.</i> [27]
		10	10 μ L droplet	2	DMF, DI water	Campos <i>et al.</i> [28]
	2-Methoxyethanol	10	Immersed	2	DMF, PBS	Kuscu <i>et al.</i> [29]
		10	Immersed	1	DMF	Xu <i>et al.</i> [30]
		10	Immersed	12	DMF, ethanol, DI water	Khan <i>et al.</i> [31]
		50	Immersed	4*	Methanol	Wang <i>et al.</i> [3]
		1	Immersed	1	DI water	Ono <i>et al.</i> [32]
		1	Immersed	1	Methanol, DI water	Zheng <i>et al.</i> [33]
		1	Immersed	2	Methanol	Kim <i>et al.</i> [34]
		100	2 μ L droplet	1	DI water	Yoo <i>et al.</i> [35]
		5	Immersed	2	-	Sethi <i>et al.</i> [36]
		5	Immersed	1	Methanol, PBS	Ohno <i>et al.</i> [37]
DMSO	CNT	10	-	1	DI water	Lopez <i>et al.</i> [38]
		10	Immersed	1	PBS	Strack <i>et al.</i> [39]

1.2. Attachment of 1-Pyrenebutanoic Acid N-Hydroxysuccinimide Ester

The non-covalent functionalisation of proteins onto a single-walled carbon nanotube using PBASE was first reported by Chen *et al.* in 2001 [14]. Two methods for protein functionalisation and immobilisation were successfully used, with the only differences being the solvent used to dissolve the PBASE powder (DMF, methanol) and the final concentration of the resulting solutions (6 mM, 1 mM respectively). The lower concentration may have been used for PBASE in methanol as PBASE powder appears to dissolve poorly in methanol at higher concentrations. Several groups directly cite Chen *et al.* when discussing functionalisation with PBASE [18], [20], [28], [33], [37]. Other groups using PBASE for graphene or carbon nanotube functionalisation do not explicitly reference Chen *et al.* in their methodology, but it is apparent they often draw on one of these two original methods. This common ancestry becomes apparent from the high frequency of methods detailing the use of 6 mM PBASE in dimethylformamide (DMF) and 1 mM PBASE in methanol, as seen in Table 1.1.

However, it is also apparent from Table 1.1 that there is a large degree of variation in the methods used for PBASE functionalisation. Various electrical characterisation, microscopy and spectroscopy techniques have been used to demonstrate successful functionalisation. Until recently, there has been little justification provided for the selection of variables used in the functionalisation procedure (e.g. length of time submerged in solvent containing PBASE), despite the wide-ranging use of this process in the literature [3], [40], [41]. This is surprising, given that the sensitivity of functionalised devices is considered to be closely related to the density of surface functionalisation [15], [42], [43]. Furthermore, a detailed investigation of PBASE functionalisation process variables has only been undertaken for graphene-based devices [3], [4], [26], [41].

Zhen *et al.*, Wang *et al.* and Mishyn *et al.* claim that carefully tuning the surface concentration of PBASE is required to avoid multilayer coverage of the graphene surface, as this negatively impacts sensing. Mishyn *et al.* use cyclic voltammetry to demonstrate that less receptor attachment to the graphene surface occurs when multiple layers of PBASE are present. However, neither group lends further support to their claim by performing analyte sensing using their functionalised graphene devices [4], [41]. In contrast, Hao *et al.* find that maximising surface coverage of PBASE results in more sensitive aptameric sensing, thus drawing the opposite conclusion [26]. The inconsistency in these recent findings mean more work is needed to understand the PBASE functionalisation process to achieve optimal biosensor sensitivity. It may also be the case that a specific functionalisation process is required for optimal sensitivity with the use of a specific type of receptor.

Once fastened to a bioreceptor via an amide or imide bond, the attachment to the linker molecule is not easily broken. However, prior to use in functionalisation processes, the NHS ester may react with any water present (hydrolysis). This reaction converts PBASE to 1-pyrenebutyric acid (PBA), leaving it unavailable to react further with amine groups [4], [15], [44]. If the amine group functionalisation is performed within a ~ 1 hour period, with a high concentration of bioreceptor used at close to neutral pH, competing hydrolysis should not have a significantly adverse impact on the functionalisation process

1. Verifying Non-Covalent Functionalisation of Carbon Nanotubes and Graphene

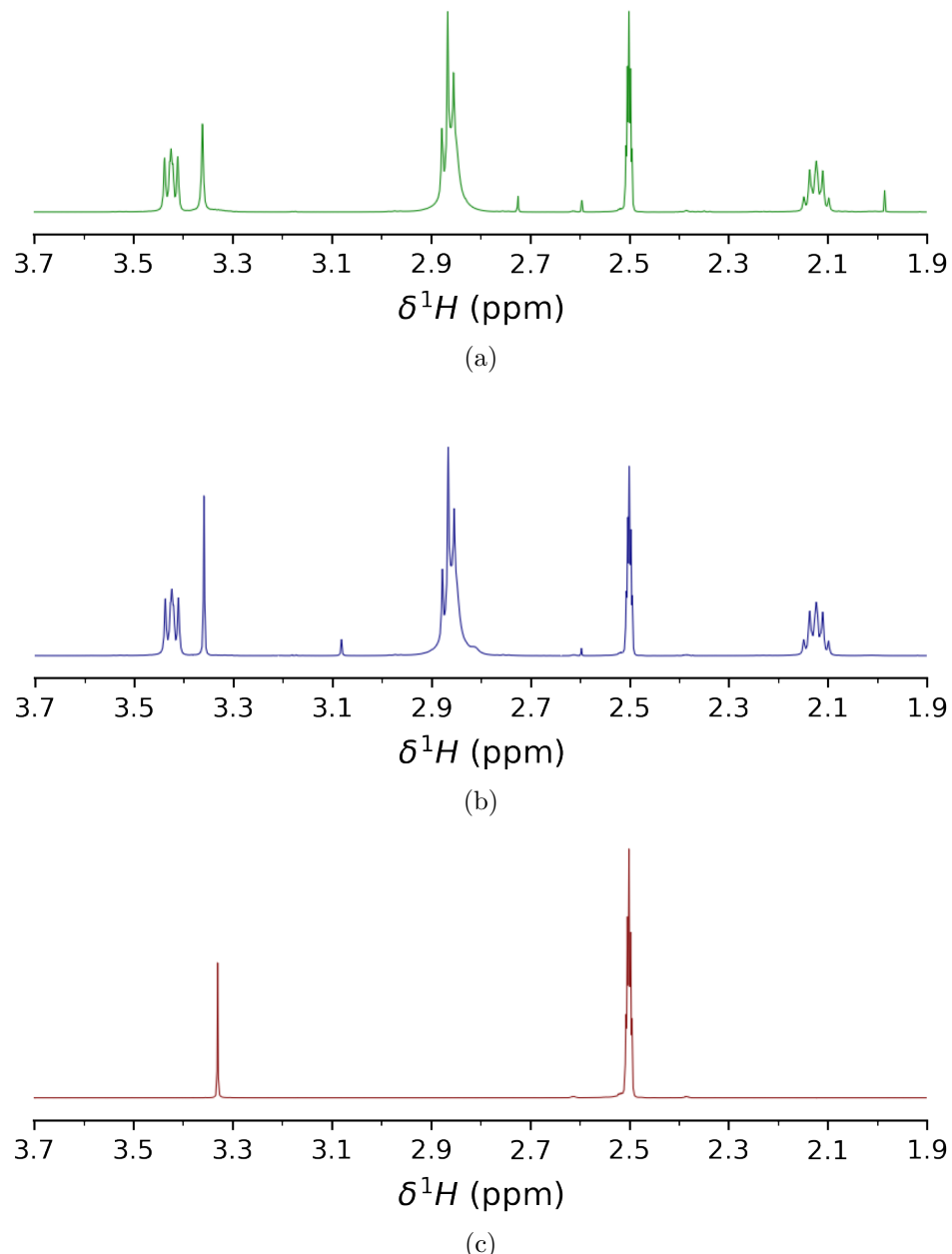


Figure 1.3.: ^1H Nuclear Magnetic Resonance (NMR) spectra, performed with DMSO-d₆ used as the NMR solvent. (a) and (b) show NMR spectrum for commercially purchased PBASE, from Sigma-Aldrich and Setareh Biotech respectively, while (c) shows the blank spectrum taken with only DMSO-d₆ present (spectra taken by Jennie Ramirez-Garcia).

1.2. Attachment of 1-Pyrenebutanoic Acid N-Hydroxysuccinimide Ester

[15]. However, if PBASE is exposed to water during storage over a significant length of time, the presence of 1-Ethyl-3-(3-dimethylaminopropyl)carbodiimide (EDC) can be used to restore the NHS ester and enable the substitution reaction to take place (see discussion of PBA/EDC in Section 1.3).

1.2.2. Examining 1-Pyrenebutanoic Acid N-Hydroxysuccinimide Ester Purity

We purchased PBASE from two suppliers, Sigma-Aldrich and Setareh Biotech. Sigma recommended DMF and methanol as suitable solvents for dissolving PBASE, alongside chloroform and dimethyl sulfoxide (DMSO). Setareh Biotech indicated methanol can be used for dissolving PBASE. The two suppliers had conflicting information for suitable storage of PBASE, with Sigma recommending room temperature storage while Setareh Biotech recommends storage of -5 to -30°C and protection from light and moisture. Given the long travel time of the PBASE samples under uncertain storage conditions, we used nuclear magnetic resonance (NMR) spectroscopy to verify the purity of the PBASE as received from each supplier. In light of the negative effect of water on PBASE, in particular we wanted to find out if any water was present in the samples.

Figure 1.3 compares the shapes of hydrogen (NMR) spectra of PBASE from each supplier when dissolved in deuterated DMSO, alongside a blank deuterated DMSO spectrum. We see both PBASE samples possess characteristic chemical shift features between $2.1 - 2.2$ ppm, $2.8 - 2.9$ ppm, and $3.4 - 3.5$ ppm. These chemical shifts roughly correspond to those seen in previous NMR spectra for PBASE [45]. The feature at 2.50 ppm represents the deuterated DMSO solvent, while the single peak between $3.3 - 3.4$ ppm represents the water present in the sample. By comparing the area of these peaks, we can estimate the amount of water originally present in the PBASE sample. The $\text{H}_2\text{O:DMSO}$ ratio is 1:7 in the blank spectrum, but $\sim 1:3$ in the provided samples, possibly indicating the introduction of water to the PBASE during production or storage. However, DMSO is strongly hygroscopic and slight differences in DMSO storage time, as well as differences in humidity during sample preparation, may have had a significant impact on this result [46]. Other impurities are also seen on both PBASE spectra, though their small size indicates they make up only a small percentage of each sample. Note that Strack *et al.* recommend leaving frozen PBASE at room temperature for 15 minutes before opening to prevent the introduction of condensation [39].

1.2.3. Electrical Characterisation

The electrical characteristics of the carbon nanotube or graphene transistor are often used to verify successful functionalisation and make a statement about the effect of chemical modification on the channel. However, this verification usually does not account for the effect of the solvent on the transistor channel. Figure 1.4a and Figure 1.4b show that by exposing a steam-deposited carbon nanotube network channel to solvents

1. Verifying Non-Covalent Functionalisation of Carbon Nanotubes and Graphene

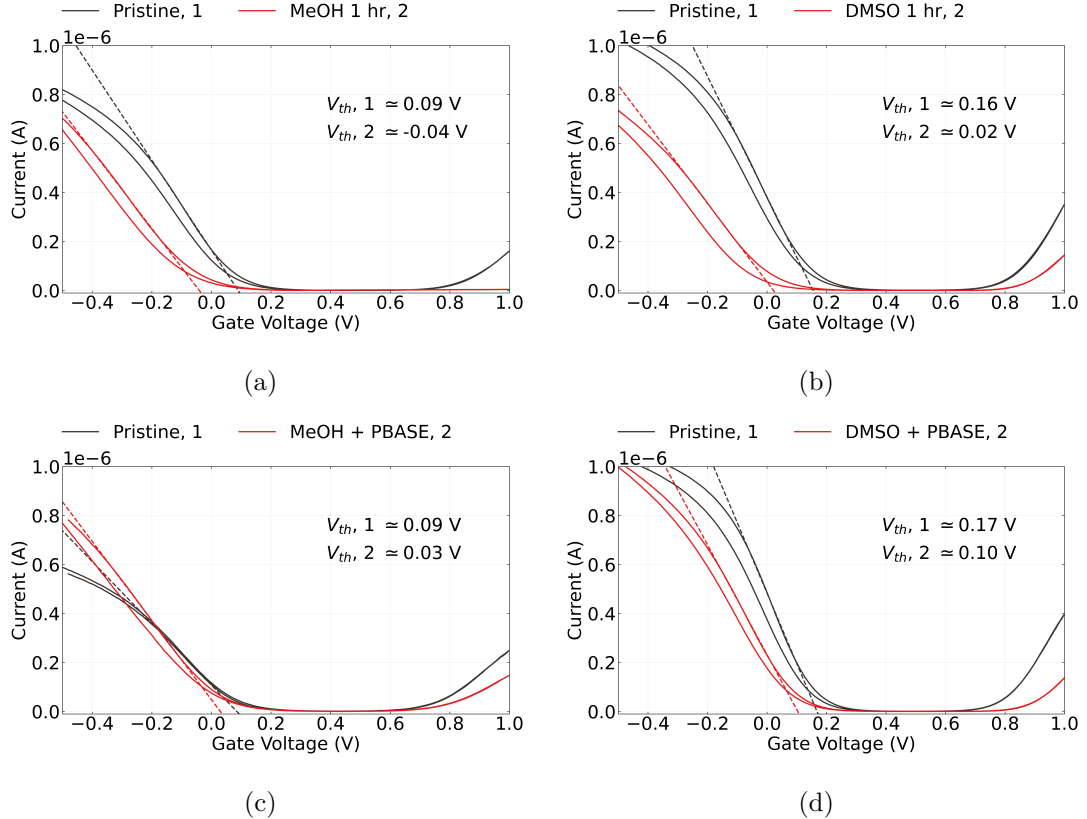


Figure 1.4.: The change in the electrical transfer characteristics of carbon nanotube transistors after being submerged in solvent for one hour and then rinsed thoroughly is demonstrated in (a) and (b), where the solvents used are methanol (MeOH) and dimethyl sulfoxide (DMSO) respectively. The change in characteristics of similar transistor channels after being submerged in these same solvents for one hour along with 1 mM PBASE then rinsed are shown in (c) and (d) respectively. Threshold voltages for each transfer characteristic are also shown.

1.2. Attachment of 1-Pyrenebutanoic Acid N-Hydroxysuccinimide Ester

commonly used in PBASE functionalisation processes (Table 1.1), such as methanol (MeOH) or dimethyl sulfoxide (DMSO), a significant negative shift in channel threshold voltage occurs even after thorough rinsing with deionised water. Besteman *et al.* reported observing a similar effect from prolonged exposure of a single carbon nanotube to dimethylformamide (DMF) [20]. It appears that the carbon nanotubes have adsorbed solvent which persists even after device cleaning. From the shape of the change in the transfer curve, it seems the residual polar solvent molecules capacitively gate the channel [47], [48].

In contrast, previous work has shown that π -stacking carbon nanotube network to PBASE does not significantly affect the channel gating and therefore the channel threshold voltage [20], [49]. Murugathas *et al.* observed a slight increase in channel conductance after PBASE functionalisation when functionalising devices with solvent-deposited CNT films. In Figure 1.4, we also observe a slight increase in channel conductance post-functionalisation for both Figure 1.4c and Figure 1.4d relative to the solvent-only case in Figure 1.4a and Figure 1.4b. It appears that the presence of PBASE molecules increases channel mobility and therefore conductance [48].

Capacitive gating results from dense coverage of adsorbed molecules on the carbon nanotube surface which have a low permittivity relative to the surrounding electrolyte [48]. The relative permittivity of MeOH and DMSO are ~ 33 [50] and ~ 47 [51] respectively, which are both much lower than the relative permittivity of phosphate buffer saline, ~ 80 [52]. From Figure 1.4a and Figure 1.4b, we find the average threshold shift values resulting from exposure to each solvent were $\Delta V = -0.15 \pm 0.03$ V and $\Delta V = -0.15 \pm 0.01$ for MeOH and DMSO respectively. The threshold voltage shifts in Figure 1.4c and Figure 1.4d from the pristine are small compared with the devices exposed to solvent only - this is likely due to the effect of increased conductance from the PBASE competing with the gating effect from the residual solvent.

This example illustrates why the use of electrical characteristics when making conclusions around a successful functionalisation process should individually take into account each substance used in the process. The qualitative presence of a change in characteristics (or lack of one) over the full process is not sufficient to make conclusive remarks about the electrical changes due to functionalisation. A full set of electrical control measurements are required for an understanding of electronic changes occurring during the functionalisation process, in the manner of Besteman *et al.* [20].

1. Verifying Non-Covalent Functionalisation of Carbon Nanotubes and Graphene

Table 1.2.: Comparison of 1-pyrenebutyric acid (PBA) functionalisation processes used for immobilisation of proteins and aptamers onto carbon nanotubes and graphene. 1-ethyl-3-(3-dimethylaminopropyl) carbodiimide hydrochloride (EDC) and NHS were co-mingled in buffer/electrolyte solution or DI water in each process - some papers used N-hydroxysulfosuccinimide instead of N-hydroxysuccinimide, and both compounds are abbreviated as NHS in this table for simplicity. Blank entries indicate there was no mention of the parameter in a particular paper. [†]PEG or PEG pyrene were used to reduce non-specific binding. ^{††}Several pyrene-based linkers were compared and PBA gave an optimal functionalisation result.

Solvent	Channel	PBA (mM)	PBA Time (hr)	EDC (mM)	NHS (mM)	EDC/NHS Time (hr)	References
DMF	Graphene	0.6	1	-	-	120	Gao <i>et al.</i> [†] [53]
		5	2	2	5	30	Mishyn <i>et al.</i> [4]
	CNT	100	3	200	-	30	Min <i>et al.</i> [54]
DI water	CNT	-	-	32	12	Overnight	Pacios <i>et al.</i> [†] [55]
Ethanol	CNT	1	1	100	100	20	Filipiak <i>et al.</i> [†] [56]
Acetonitrile	Graphene	1	1	400	100	60	Tong <i>et al.</i> ^{††} [57]
Borax solution	CNT	2	24	2.5	-	1080	Liu <i>et al.</i> [†] [58]
DMSO	Graphene	5	1	50	50	90	Fenzl <i>et al.</i> [59]

1.3. Attachment of 1-Pyrenebutyric Acid

1.3.1. Comparing Attachment Methods

Another linker molecule that can be used to attach receptor molecules to a carbon nanotube or graphene channel is 1-pyrenebutyric acid (PBA). As with PBASE, the pyrene group of PBA has a π interaction with the carbon rings of the channel surface. It is possible to react PBA with 1-ethyl-3-(3-dimethylaminopropyl) carbodiimide hydrochloride (EDC or EDAC) to form an *O*-acylisourea intermediate, which can then react with an amine group on a biomolecule and form an amide bond [60], [61]. The water solubility of EDC means that, unlike PBASE, it is possible to functionalise with EDC dissolved in water rather than in an organic solvent. However, like PBASE, EDC and the *O*-acylisourea intermediate are prone to hydrolysis, especially in acidic conditions. Therefore, like PBASE, it should be stored at -20°C , and warmed to room temperature to prevent condensation build-up, since exposure to condensation will hydrolyse the reagent [61]. Furthermore, by adding N-Hydroxysuccinimide (NHS) or N-hydroxysulfosuccinimide (sulfo-NHS) to the reaction vessel, PBASE is formed as an active intermediate, which is less prone to hydrolysis and increases the PBA/EDC reaction yield [60]–[62].

From comparing Table 1.1 and Table 1.2, we see that PBASE is more widely used for non-covalent functionalisation than PBA/EDC. As was the case for PBASE, there are a wide range of process variables used for the functionalisation process, with little justification used for variables chosen. Also notable is the frequent use of polyethylene glycol (PEG) or pyrene-PEG for prevention of non-specific binding (see [?@sec-non-specific-binding](#) for further discussion of NSB). Despite being less widely used, Mishyn *et al.* state a preference for the use of PBA/EDC over PBASE, as they found it was less prone to hydrolysis and gave a larger reaction yield when binding ferrocene to graphene [4]. A potential downside of using PBA/EDC for protein immobilisation is that EDC has numerous ways of interacting with proteins, and not all of these are necessarily desirable. The addition of NHS may also cause processing issues, such as precipitation of the reaction compound [61]. The greater range of process variables involved in the functionalisation also adds to the complexity of accurately reproducing past results.

1.3.2. Raman Spectroscopy

Raman spectroscopy was used to verify the attachment of PBA to a carbon nanotube network film. The carbon nanotube films used for verifying pyrene attachment were solvent-deposited, as highly-bundled devices were found to give a better optical signal-to-noise ratio, as discussed in [?@sec-pristine-raman](#). Droplets of DMSO solution were placed on three (solvent-deposited) carbon nanotube films taken from the same wafer. The DMSO solution on one film contained 5mM PBA, the solution on another film contained 5 mM PBASE, and the DMSO on the final film contained no linker

1. Verifying Non-Covalent Functionalisation of Carbon Nanotubes and Graphene

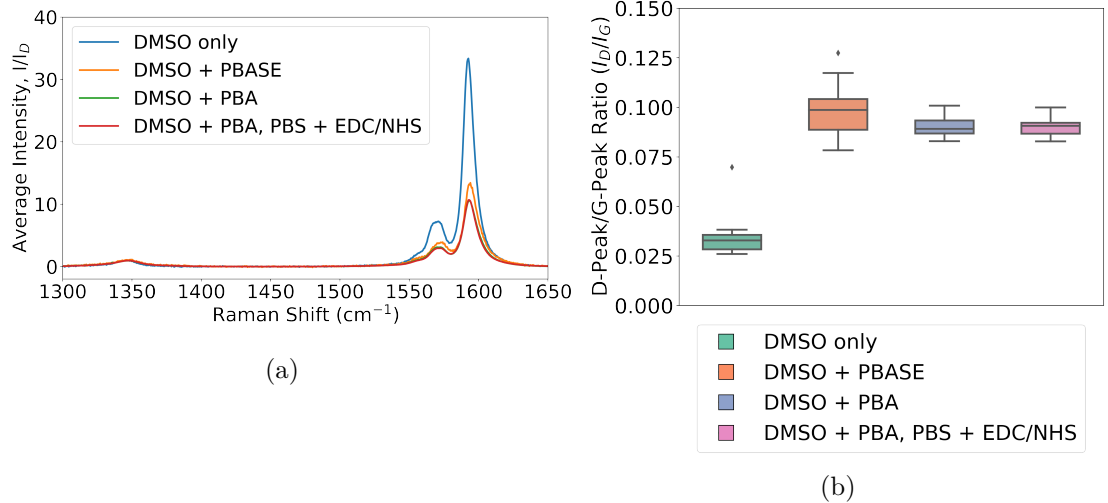


Figure 1.5.: Each spectrum shown in (a) corresponds to the average intensity across nine Raman spectra at different locations across a selection of chemically-modified carbon nanotube films. Each spectrum has been normalised so that $I_D = 1$ (D-peak maximum is unity). (b) shows the distribution of D-band peak to G-band peak ratio (I_D/I_G) calculated for each of the nine locations on each film.

molecule. After incubation for 1 hour, films were rinsed for 15 s with DMSO, then for 15 s with IPA to remove excess DMSO while avoiding hydrolysis of the PBASE. Raman spectroscopy was performed on the films in the manner outlined in ?@sec-raman-characterisation. The PBA-exposed film was further exposed to 20 mM EDC and 40 mM NHS in 1XPBS electrolyte for 30 minutes, and a second Raman spectra was taken for this film. The average intensity of Raman shift for each film measurement set is shown in Figure 1.5a. The distribution of I_D/I_G ratio across all nine Raman spectra from each film measurement set is shown in Figure 1.5b.

There is a $\sim 3\times$ increase in the intensity ratio I_D/I_G for both the films modified with PBASE and PBA compared to the film which was only exposed to DMSO. Previous works have found that a change in the intensity ratio indicates successful π -stacking on the carbon nanotube surface, as it indicates surface modification of the carbon nanotubes has occurred [63], [64]. Wei *et al.* found functionalisation with PBASE altered the ratio by a factor of $\sim 1.5\times$, while Lan *et al.* found that functionalisation with PBA altered the ratio by a factor of $\sim 0.8\times$. The reason for the large difference between results is not immediately clear, but may result from the significant differences in the pristine composition and morphology of carbon nanotube networks used in each publication, and differences in the functionalisation method used. We see from Figure 1.5b that across all scan locations, there is significant overlap between I_D/I_G measurements for both PBA and PBASE. Furthermore, after further functionalisation of the PBA-modified film with EDC/NHS, subsequent Raman measurements of the film do not differ significantly to

1.3. Attachment of 1-Pyrenebutyric Acid

measurements taken before adding the EDC/NHS. These results indicate that presence of the NHS ester has little effect on the Raman shift. Therefore, it should be clarified that Raman spectroscopy cannot be used to distinguish between the presence of PBA and PBASE on the device surface.

1.3.3. Electrical Characterisation

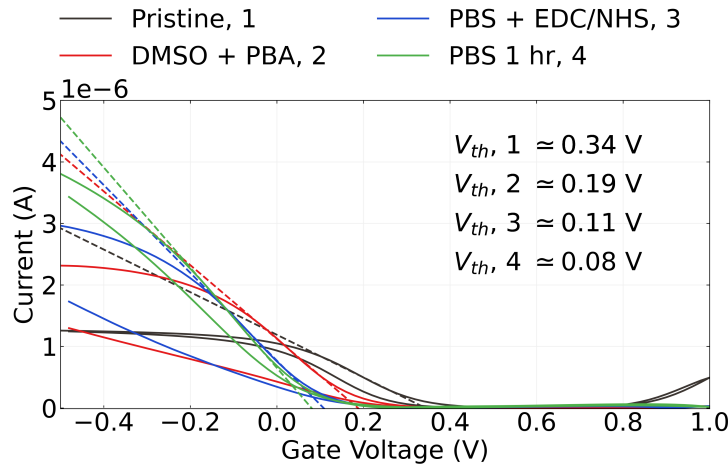


Figure 1.6.: Electrical transfer characteristics of a carbon nanotube transistor before functionalisation, after being submerged in DMSO containing 5 mM PBA for 1 hour, after being submerged in 1XPBS containing 20 mM EDC and 40 mM NHS for 30 min, then after being submerged in fresh 1XPBS for 1 hour. Threshold voltages for each transfer characteristic are also shown.

Figure 1.6 shows the transfer characteristics of a carbon nanotube transistor at various stages of a PBA/EDC functionalisation, where a excess of N-hydroxysuccinimide (NHS) was added alongside EDC. The device used was fabricated in Jan 2022, where the carbon nanotubes were solvent-deposited. The PBA was dissolved in DMSO, and the device channels were exposed to this solution for 1 hour. Subsequently, it was rinsed with 1XPBS and exposed to 20 mM EDC and 40 mM NHS in 1XPBS electrolyte for 30 minutes. We can compare Figure 1.6 to Figure 1.4 for a better understanding of the result of both the PBASE and PBA/EDC functionalisation methods. The threshold shift with the addition of 5 mM PBA in DMSO for 1 hour is equivalent to the shift seen when only DMSO is added, $\Delta V = -0.15$ V. The lack of a significant threshold shift is a result of pyrene having a neutral charge state, and any contributions from the charged carboxyl group being screened from the carbon nanotube sidewalls by surrounding water molecules [65]. However, as in the case of the addition of PBASE, there also appears to be an increase in hole mobility, which may be due to the pyrene groups increasing

1. Verifying Non-Covalent Functionalisation of Carbon Nanotubes and Graphene

connectivity within the carbon nanotube network [49]. When EDC/NHS is added, a further increase in mobility of channel holes is seen [48].

1.4. Attachment of PEGlyated Pyrene-Based Linkers

1.4.1. Pyrene-NTA, Pyrene-Biotin and PEGylation

Through chemical coupling/conjugation, it is possible to replace the NHS ester group on PBASE with other groups that can undergo binding reactions with proteins. These groups do not suffer the same drawback of being readily hydrolysed as PBASE does. For example, PBASE can be modified with Na,Na -Bis(carboxymethyl)-L-lysine hydrate (also known as N-(5-Amino-1-carboxypentyl)iminodiacetic acid, AB-NTA) to produce pyrene-nitrilotriacetic acid (pyrene-NTA). The attached NTA group is able to chelate with metal ions such as Cu^{2+} or Ni^{2+} , which then can then coordinate with polyhistidine-tags attached to a protein [66]–[68]. Use of Cu^{2+} ions over Ni^{2+} gives stronger histidine bonding and less non-specific adsorption [68]. Functionalisation using the NTA- Ni^{2+} chemistry was successfully used to attach mammalian odorant receptors to a single carbon nanotube for detection of eugenol vapour in real-time [69]. Pyrene-biotin (pyrene butanol biotin ester) can also be produced for attaching avidin or streptavidin [66]. As avidin and streptavidin are tetrameric, they can be attached to both pyrene-biotin and biotinylated avi-tagged proteins simultaneously via strong non-covalent bonding, therefore linking the transducer and receptor [70]–[73]. As the presence of his-tags and avi-tags on proteins can be readily controlled, these methods offer improved specificity and directionality over the traditional amide bonding seen earlier.

It is also possible to attach polyethylene glycol (PEG) chains to a pyrene group and modify them with reactive groups such as NTA and biotin to attach proteins in the manner outlined in the previous paragraph [74], [75]. Once modified with PEG, the water solubility of pyrene linkers increases, making it possible to perform a full functionalisation procedure exclusively in aqueous solution [74]. By setting the length of the PEG chain, the size of the linker molecule can be controlled - selection of a short chain is important for ensuring attached receptors remain within the Debye length of the transducer [52]. Functionalisation of a graphene transducer with pyrene-PEG-biotin has previously been used to bind streptavidin to a graphene field-effect transistor device [76]. The PEGlyated linkers used in the following sections were purchased pre-prepared. Pyrene-PEG-NTA (2 kDa) was purchased from Nanocs, while pyrene-PEG-FITC (2 kDa, 10 kDa), pyrene-PEG-rhodamine (3.4 kDa), mPEG-Pyrene (Pyrene-PEG, 10 kDa) and pyrene-PEG-biotin (10 kDa) were purchased from Creative PEGworks.

1.4. Attachment of PEGlyated Pyrene-Based Linkers

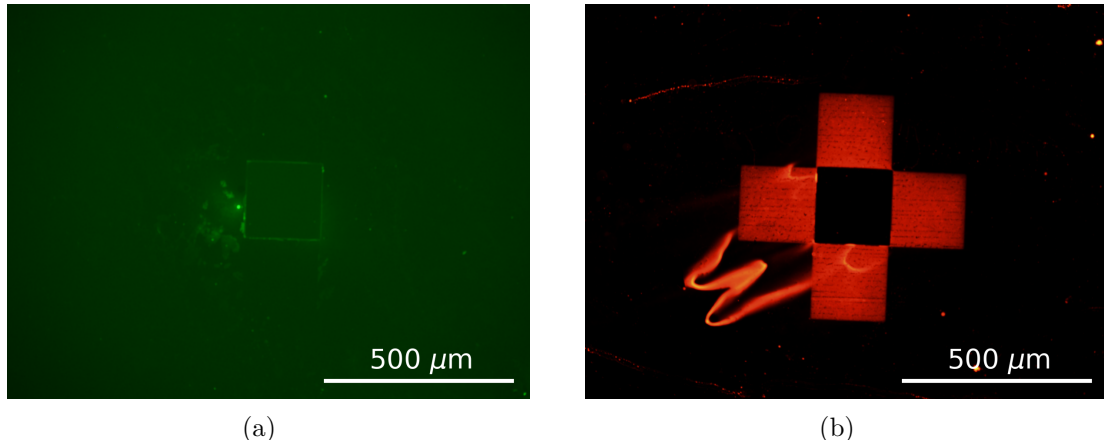


Figure 1.7.: Four $200\text{ }\mu\text{m} \times 200\text{ }\mu\text{m}$ graphene squares modified with FITC in (a), and with Rhodamine B in (b). In (a), an FITC filter and 6.5 s exposure time was used, and in (b) a Texas Red filter and 1.4 s exposure time was used.

1.4.2. Fluorescence Characterisation with Pyrene-PEG-FITC

To understand the attachment of PEGlyated pyrene-based linkers to the carbon nanotube or graphene surface, we used pyrene-PEG modified with fluorescein isothiocyanate, a widely-used fluorescent probe which does not specifically interact with carbon rings. Figure 1.7 gives a comparison of the presence of FITC and Rhodamine B with four $200\text{ }\mu\text{m} \times 200\text{ }\mu\text{m}$ graphene squares. There is a much stronger contrast between the graphene squares and the background after functionalisation with Rhodamine B, showing a clear, specific interaction between Rhodamine B and graphene. It has previously been determined that the benzene rings of rhodamine π -stack with carbon rings [77]. As we want to measure the attachment of pyrene, not the fluorescent modifier, we use FITC instead of Rhodamine B. Figure 1.8 shows various concentrations of pyrene-PEG-FITC dissolved in 1XPBS, which is used for fluorescence characterisation in this section.

The functionalisation of graphene devices with pyrene-PEG-FITC was performed as follows:

1. 1 mM pyrene-PEG-FITC was prepared in ethanol by sonication for 1 minute then vortex mixing for 10-15 minutes, to fully dissolve the pyrene-PEG-FITC (Note: pyrene-PEG-FITC is stored frozen, should be defrosted under vacuum 15 minutes before use).
2. Unencapsulated device was rinsed with acetone and IPA, then nitrogen dried.
3. The device was then fully submerged in pyrene-PEG-FITC/ethanol solution for 20 minutes.

1. Verifying Non-Covalent Functionalisation of Carbon Nanotubes and Graphene

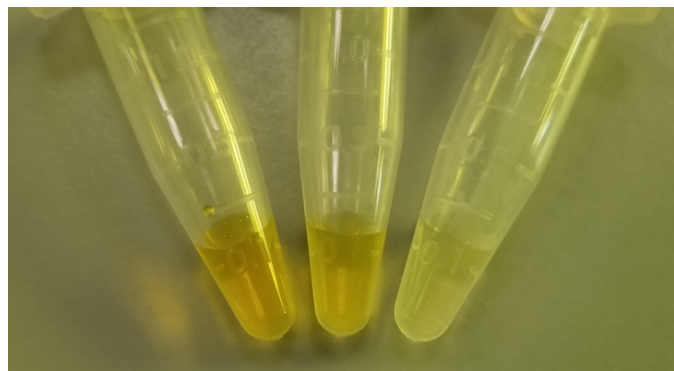


Figure 1.8.: Microcentrifuge tubes containing various concentrations of 10 kDa pyrene-PEG-FITC in solution (1 mM, 0.1 mM and 0.01 mM left to right)

4. After 20 minutes, device was rinsed for 30 s with ethanol, then acetone, IPA and nitrogen dried.

Fluorescence images of the unencapsulated graphene devices successfully functionalised with pyrene-PEG-FITC are shown in Figure 1.9. The dark regions are the gold electrodes, and the bright green region is the graphene channel. It is noticeable that some variation in fluorescence is seen between channels, indicating the quality of functionalisation may vary across the channels of a device. Some of the difficulties encountered when investigating functionalisation with pyrene-PEG-FITC are outlined in Section 1.6.

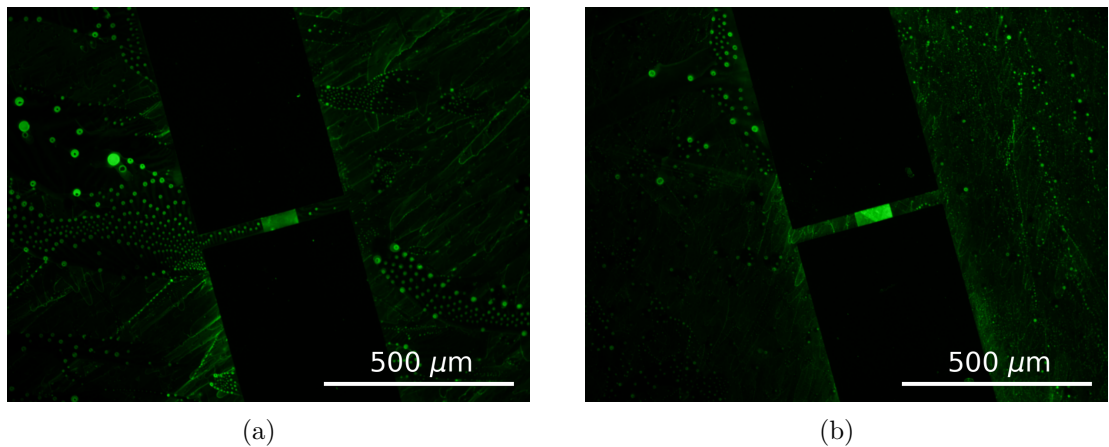


Figure 1.9.: Fluorescence images of an unencapsulated graphene channel after functionalisation with 1 mM pyrene-PEG-FITC in ethanol, taken using an FITC filter and a 1 s exposure time, where (a) is channel 2 of the device and (b) is channel 7.

1.4.3. Electrical Characterisation with Pyrene-PEG

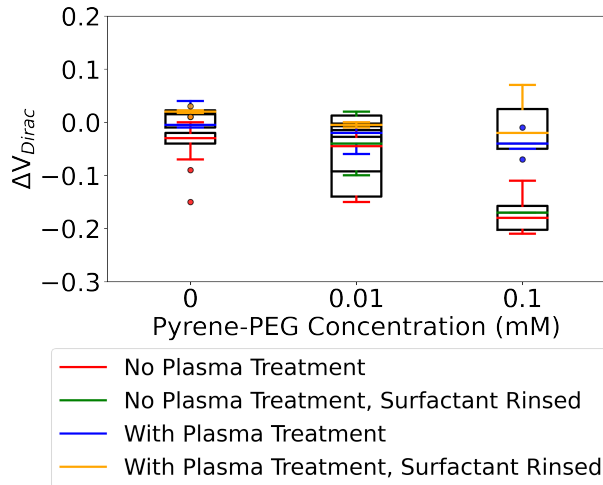


Figure 1.10.: (Major) Dirac voltage shifts of graphene field-effect transistors after functionalisation with various concentrations of pyrene-PEG dissolved in 1XPBS, as well as after being cleaned with m-surfactant solution. Measurements corresponding to each concentration are of three different device channels from a single device measured four times, where the device was rinsed with 1XPBS between each measurement.

Figure 1.10 compares the electrical characteristics of graphene transistor channels before and after functionalisation with various concentrations of pyrene-PEG, showing the magnitude in shift of the (major) Dirac point. Graphene devices used were fabricated before Nov 2022. 2 mM Pyrene-PEG was dissolved in 1XPBS using a vortex mixer for 10 min at 1000 rpm until fully dissolved, then diluted in series to 1 mM, 0.1 mM, and 0.01 mM in 1XPBS. Plasma treated devices were treated with 5W oxygen plasma for 15 s at 350 mTorr before functionalisation. 2 μ L solution was placed on each device channel for 1 hour, covered with a glass dish and in the presence of wet tecwipes to keep the environment humid. Devices were then rinsed in 1XPBS for 30 s before measurements were taken. Surfactant rinsing involved placing functionalised devices in m-CNT dispersion solution for 5 minutes at 70°C, periodically agitating the solution with a pipette, then rinsing the devices with DI water, ethanol, acetone, IPA and finally nitrogen drying them.

As in the case of PBASE and PBA on carbon nanotubes, the neutral charge of pyrene means there is no significant Dirac shift when the plasma treated devices are successfully functionalised with pyrene-PEG [65]. Interestingly, however, when the devices are not plasma treated before functionalisation, there is a significant Dirac shift at higher concentrations of pyrene-PEG. As we expect little or no graphene surface coverage to result from aqueous functionalisation without a plasma pre-treatment, as demonstrated in Section 1.4.2, we can therefore assume this shift is due to attachment of pyrene-PEG

1. Verifying Non-Covalent Functionalisation of Carbon Nanotubes and Graphene

to the small region of silicon dioxide not covered by encapsulation which borders the channel. Furthermore, Section 1.4.2 shows us that even after plasma treatment, the SiO₂ surface will still interact with pyrene-PEG upon functionalisation. Oxygen plasma treatment is known to make the graphene layer permeable to water, and therefore it is likely the SiO₂ surface below the graphene is also coated with pyrene-PEG after plasma treatment [78]. Therefore, it appears the Dirac shift results from a difference in pyrene-PEG surface coverage when comparing the SiO₂ surface next to the graphene channel and the SiO₂ below the graphene channel. The physical mechanism linking these two factors is currently unclear.

1.5. Verifying Linker-Receptor Attachment

1.5.1. Functionalisation with GFP-OR Nanodiscs using PBASE

To verify the formation of amide (or imide) bonds between PBASE and the odorant receptors (ORs) contained within nanodiscs, a fluorescent biomarker was directly attached to the odorant receptors for detection with fluorescence microscopy. The biomarker used was the *Aequorea victoria* green fluorescent protein (GFP). As far as we know, this is the first time fluorescence has been used to verify the successful attachment of odorant receptor nanodiscs to a carbon nanotube network.

The functionalisation of unencapsulated carbon nanotube devices (steam-deposited, fabricated after June 2023) with PBASE and GFP-OR Nanodiscs was performed as follows:

1. The device was vacuum annealed for 1 hour at 150°C.
2. The device was exposed to UV light for 1 minute, placed in AZ® 326 developer for 3 minutes, then rinsed with acetone, isopropanol and nitrogen dried (Note: Steps 1 & 2 were added to ensure any residual photoresist on the channel was removed before functionalisation, see subsequent discussion).
3. A solution of 1 mM PBASE (Setareh Biotech) in methanol prepared by fully dissolving 2 mg PBASE in 5 mL methanol by vortex mixing at 1000 rpm in a dark room (Note: PBASE was stored at -18°C for 18 months prior to use, and was thawed under vacuum for 15 minutes in dark conditions before opening)
4. The device was then rinsed with methanol, fully submerged in ~ 1 mL of PBASE in methanol solution and left covered with parafilm for 1 hour, then rinsed with methanol for 15 s, rinsed with 1XPBS for 15 s and nitrogen dried to remove residual PBASE.
5. The device was left dry and in darkness while collecting the GFP-OR nanodiscs from the -80°C freezer.

1.5. Verifying Linker-Receptor Attachment

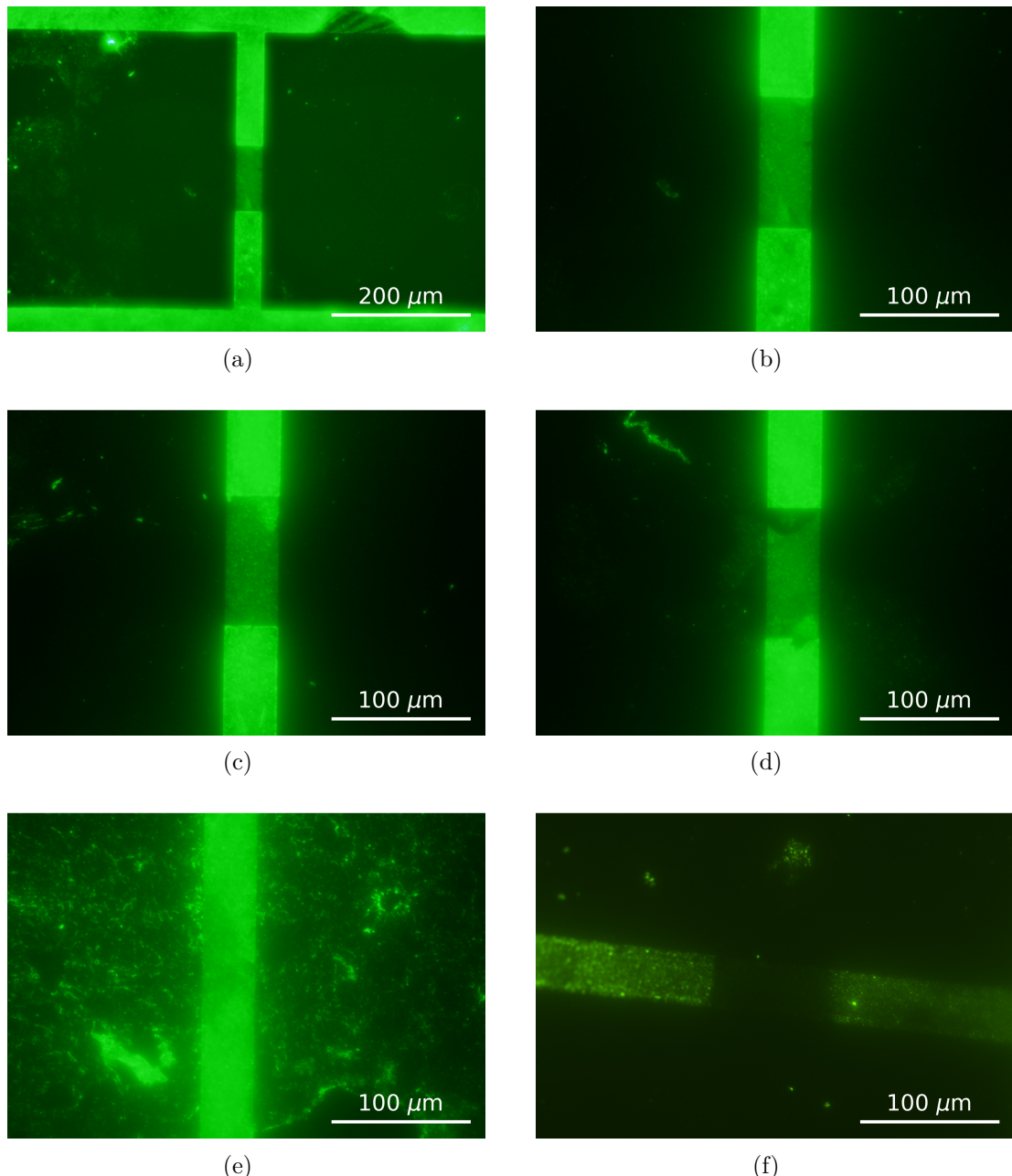


Figure 1.11.: Fluorescence images of an unencapsulated carbon nanotube network channel after functionalisation with 1 mM PBASE in methanol, followed by 10 μ L:2 mL GFP-OR43b nanodiscs.(a) and (b) show channel 1 of the device, (c) shows channel 2, (d) shows channel 3 and (e) shows channel 6. The image in (f) was taken of a separate device functionalised using 0.1 mM PBASE. All images were taken using an GFP filter and a 10 s exposure time.

1. Verifying Non-Covalent Functionalisation of Carbon Nanotubes and Graphene

6. 10 μL GFP-OR nanodiscs (batch number ND-GFP-OR43b-0002, prepared 12 months earlier) was diluted in 2 mL 1XPBS (Note: The full 2 mL was used to flush out the nanodisc vial when preparing the nanodisc solution, with successive additions and subtractions of 50 μL 1XPBS into and from the vial).
7. The device was submerged in the GFP-OR43b nanodisc solution and left covered with parafilm for 1 hour, then rinsed with 1XPBS for 15 s.
8. For fluorescence microscopy, the device was briefly rinsed with DI water and nitrogen dried to remove salt residue from the 1XPBS.

Fluorescence images of the unencapsulated carbon nanotube devices successfully functionalised with GFP-OR43b nanodiscs using PBASE are shown in Figure 1.11 (a)-(e).

As in Section 1.4.2, dark regions are the gold electrodes. Immediately, we notice that there is significant attachment of GFP-OR43b nanodiscs to the silicon dioxide surface. As this device has been annealed, UV exposed and developed before functionalisation, this non-specific attachment is unlikely to be interaction with residual photoresist (see Section 1.6.2). Instead it appears that the pyrene, nanodiscs or both are directly interacting with the silicon dioxide surface. Fluorescence in the channel region in Figure 1.11 (a)-(e) indicates GFP-OR43b nanodiscs are present on or around the carbon nanotubes. The fluorescence brightness was consistent across four out of eight channels on the 1 mM PBASE functionalised device. The other four channels looked similar to Figure 1.11e, where nanodiscs appeared to be present in excess on both the channel, SiO_2 , and even on the gold electrodes. This is an indication that the concentration of GFP-OR43b used should be lowered further for a more consistent functionalisation.

Figure 1.11f shows that a lowered concentration of PBASE leads to a channel region with no visible fluorescence (with a 10 s exposure time). This indicates that the PBASE solution used to incubate the device must be sufficiently concentrated for odorant receptors to interact with the channel region, indicating that a specific interaction is occurring between PBASE and the GFP-OR43b in Figure 1.11 (a)-(e). Further evidence for successful functionalisation is provided in Section 1.6.3.

1.5.2. Functionalisation with GFP-OR Nanodiscs using Pyrene-PEG-NTA

Pyrene-PEG-NTA was also used to attach the green fluorescent protein tagged odorant receptors through attaching to their histidine tag via the mechanisms outlined in Section 1.4.1. As nanodiscs as well as odorant receptors have attached amine groups (see [?@sec-artificial-membranes](#)), even nanodiscs which do not contain the receptor required for sensing can attach to the carbon nanotubes in the presence of PBASE linker. However, the nanodiscs used here possessed no histidine tag. Therefore, successful GFP-OR Nanodisc attachment via a histidine bonding process indicates odorant

1.5. Verifying Linker-Receptor Attachment

receptors, rather than nanodisc membranes, have specifically attached to the carbon nanotube network.

The following procedure was used to functionalise unencapsulated carbon nanotube devices (steam-deposited, fabricated after June 2023) with pyrene-PEG-NTA and GFP-OR Nanodiscs:

1. The device was vacuum annealed for 1 hour at 150°C.
2. The device was exposed to UV light for 1 minute, placed in AZ® 326 developer for 3 minutes, then rinsed with acetone, isopropanol and nitrogen dried (Note: Steps 1 & 2 were added to ensure any residual photoresist on the channel was removed before functionalisation, see subsequent discussion).
3. A solution of 100 μ M Pyrene-PEG-NTA (Nanocs) in ethanol was prepared by fully dissolving 1 mg Pyrene-PEG-NTA in 5 mL ethanol by sonicating for 1 minute in a dark room (Note: Pyrene-PEG-NTA was stored at -18°C for 6 months prior to use, and was thawed under vacuum for 15 minutes in dark conditions before opening; the solution was left at 4°C for a week before use).
4. 10 mL of 10 mM CuSO₄ in 1XPBS was prepared by dissolving CuSO₄ powder in 1XPBS by vortex mixing for 15 minutes.
5. After vortex mixing Pyrene-PEG-NTA in ethanol solution at 1000 rpm for 10 minutes, the Pyrene-PEG-NTA solution was diluted to 1 μ M in ethanol by placing 100 μ L into 9.9 mL ethanol.
6. The device was then rinsed with acetone, IPA and nitrogen dried, fully submerged in 10 mL of 1 μ M Pyrene-PEG-NTA in ethanol solution and left covered with parafilm for 15 minutes, then rinsed with ethanol for 15 s, rinsed with 1XPBS for 15 s and nitrogen dried to remove residual Pyrene-PEG-NTA.
7. The device was then placed in 10 mL of CuSO₄ in 1XPBS and covered with parafilm for 1 hour to coordinate Cu²⁺ with NTA, then rinsed 15 with 1XPBS (Note: NiSO₄ can be used as an alternative)
8. 10 μ L GFP-OR nanodiscs were diluted in 10 mL 1XPBS (batch number ND-GFP-OR43b-0002, prepared 12 months earlier and stored at -80°C) .
9. The device was submerged in the GFP-OR43b nanodisc solution and left covered with parafilm for 30 minutes, then rinsed with 1XPBS for 15 s.
10. For fluorescence microscopy, the device was rinsed with DI water for 1 minute and nitrogen dried to remove salt residue from the 1XPBS.

Fluorescence images of the unencapsulated carbon nanotube devices successfully functionalised with GFP-OR43b nanodiscs using Pyrene-PEG-NTA are shown in Figure 1.12. Similar non-specific attachment to the silicon dioxide as in Section 1.5.1 is seen, but there

1. Verifying Non-Covalent Functionalisation of Carbon Nanotubes and Graphene

is clear attachment of green fluorescent protein-modified odorant receptors in the channel, indicating specific attachment via histidine.

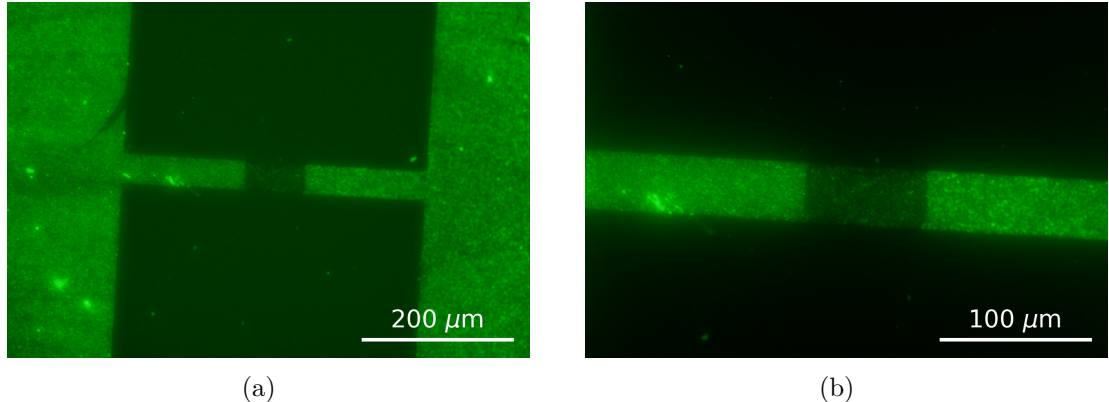


Figure 1.12.: Fluorescence images of an unencapsulated carbon nanotube channel after functionalisation with 10 μL :10 mL GFP-OR43b nanodiscs using pyrene-PEG-NTA and Cu^{2+} . Images (a) and (b) are of channel 4, and were taken using an GFP filter and a 10 s exposure time.

1.6. Overcoming Issues with Functionalisation

1.6.1. Hydrophobicity of Carbon Nanotubes and Graphene

A second obstacle encountered when verifying the attachment of pyrene-based linker was the hydrophobicity of carbon nanotubes and graphene. As seen in Figure 1.13a, when a graphene film was submerged in 1XPBS solution containing pyrene-PEG-rhodamine (PPR), the graphene would neither interact with the pyrene or the rhodamine. Instead, we see that the pyrene-PEG-rhodamine interacted exclusively with the surrounding silicon dioxide substrate. We assume that this occurs due to the highly hydrophobic graphene surface repelling surrounding solution, preventing π -stacking from occurring. However this hydrophobicity is not intrinsic to graphene (or to carbon nanotubes), and instead results from a hydrocarbonaceous layer which forms on the graphene (or carbon nanotube) surface when exposed to air [79], [80]. Treatment with oxygen plasma at 5 W for 15 s has previously been found to remove this hydrocarbonaceous layer, restoring the intrinsic hydrophilicity of graphene [81]. Furthermore, storing the graphene surface in DI water rather than air prevents the reemergence of the hydrocarbon layer [79].

Treatment of an unencapsulated carbon nanotube network device at 5 W for 15 s at 300 mTorr greatly reduced the contact angle of a water droplet placed on the device surface, shown inset in Figure 1.13 before and after plasma treatment. A graphene film was then functionalised with pyrene-PEG-rhodamine in 1XPBS in the same manner as for the film in Figure 1.13a, except with the same plasma treatment performed on the

1.6. Overcoming Issues with Functionalisation

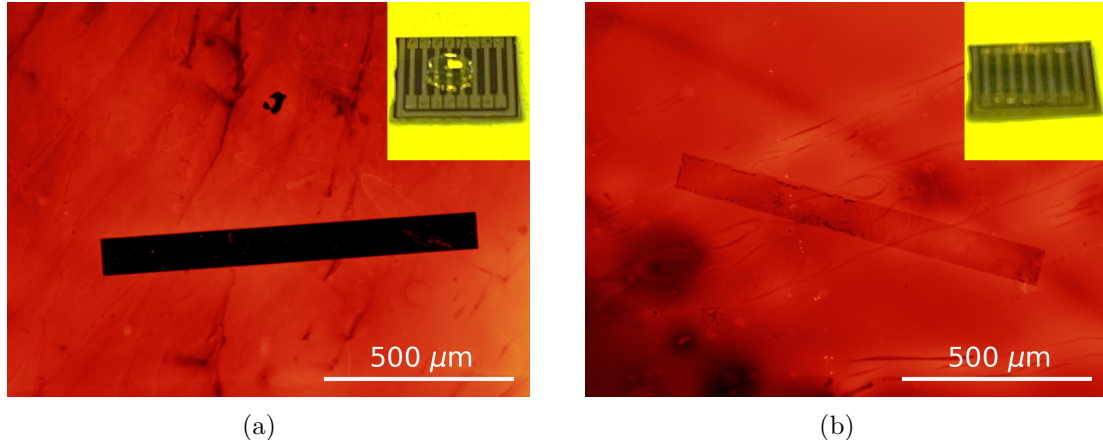


Figure 1.13.: Fluorescence images of a $1000 \mu\text{m} \times 100 \mu\text{m}$ graphene channel after functionalisation with 1 mM pyrene-PEG-rhodamine in 1XPBS, taken using an Texas Red filter and a 1.8 s exposure time. The graphene film in (a) was not oxygen plasma cleaned before functionalisation, while the graphene film in (b) was oxygen plasma cleaned at 5 W for 15 s at 300 mTorr pressure immediately before functionalisation. Insets show a $10 \mu\text{L}$ droplet placed on an unencapsulated carbon nanotube device before (a) and after (b) the same oxygen plasma treatment procedure.

film less than 1 minute before functionalisation. The result is shown in Figure 1.13b. We see that the graphene now interacts with the pyrene-PEG-rhodamine. These results both indicate that the plasma treatment is increasing the hydrophilicity of the device surface, improving the ability of pyrene-PEG-rhodamine to π -stack with graphene. The disadvantage of this procedure is that the plasma cleaning introduces defects to the graphene surface which may be undesirable for device electrical behaviour. It was often found that devices functionalised in this manner had their conductance drop significantly after functionalisation, even though plasma treatment itself did not significantly alter device conductance. Initial functionalisation in solvent was therefore preferred, as it did not require a plasma cleaning step for successful attachment.

1.6.2. Photoresist Contamination

An early difficulty encountered when characterising Pyrene-PEG-FITC attachment (PPF) via fluorescence microscopy is the presence of photoresist. Figure 1.14a shows an fluorescence image of a carbon nanotube device channel encapsulated with SU8, taken with a FITC filter. The photoresist itself is seen to fluoresce due to its photoactive component [82], and therefore a different type of encapsulation would need to be used when verifying channel attachment via fluorescence after encapsulation. Alternative encapsulation methods which can be used with fluorescence microscopy are discussed in

1. Verifying Non-Covalent Functionalisation of Carbon Nanotubes and Graphene

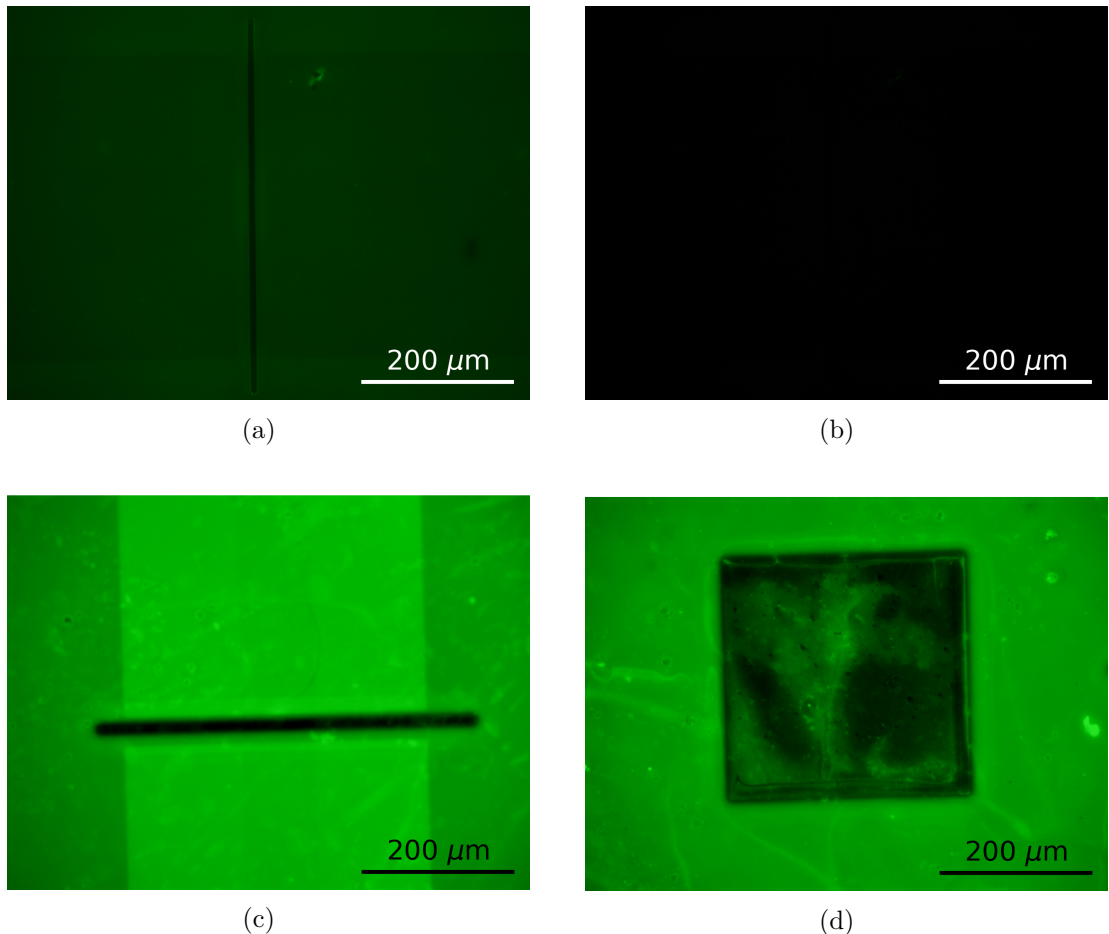


Figure 1.14.: A fluorescence image of a carbon nanotube device encapsulated with SU8 using the pre-2023 mask is shown in (a) using a 4.5 s exposure time. An image of the same region on this device taken using a shorter exposure time (0.35 s) is shown in (b). With the same exposure time as in (b), (c) shows a SU8-encapsulated channel after modification with an aqueous solution of 1 mM Pyrene-PEG-FITC, while (d) shows an SU8-coated CNT film where a $320 \mu\text{m} \times 320 \mu\text{m}$ region of SU8 has been photolithographically removed to expose the CNTs in that region. All images were taken using an FITC filter.

1.6. Overcoming Issues with Functionalisation

?@sec-future-work. We also see that the pyrene-PEG-FITC appears to interact with the SU8 surface. Figure 1.14b and Figure 1.14c were taken using the same microscope settings (filter, ISO, contrast, exposure time), yet the SU8 exposed to PPF appears much brighter than the pristine SU8. Furthermore, once exposed to PPF we can clearly see photoresist residue on a carbon nanotube film, as shown in Figure 1.14d. The presence of photoresist residue is not only undesirable for sensing purposes but also interferes with the use of fluorescence microscopy for functionalisation verification. Approaches to dealing with photoresist contamination are outlined in Section 1.5.

1.6.3. Interactions between Substrate and Pyrene(-PEG)

Another issue that arose when verifying surface functionalisation is that pyrene-PEG interacts with silicon dioxide, making it difficult to discern whether the pyrene group is interacting in a specific manner with the graphene or carbon nanotube film. This can be seen for pyrene-PEG-rhodamine in Figure 1.13, and also for pyrene-PEG-FITC in Figure 1.15a. It was confirmed that pyrene-PEG was interacting with silicon dioxide rather than residual photoresist or nanomaterial by performing a pyrene-PEG-rhodamine functionalisation on pristine silicon dioxide, shown in Figure 1.15b. The supplier suggested that we thoroughly rinse the surface with surfactant to remove weakly-bound pyrene-PEG-FITC attached to the silicon dioxide, while preserving the pyrene-PEG-FITC strongly attached via π -stacking to the graphene or carbon nanotube film [83]. The following process was then used to remove pyrene-PEG-FITC from the silicon dioxide: the film was rinsed with DI water for 30 s, then placed in m-CNT dispersion solution (NanoIntegris) for 5 minutes at 70°C while agitating with a pipette, and finally rinsed with DI water, ethanol, acetone, IPA and nitrogen dried. The results of this thorough cleaning process are shown in Figure 1.15c and Figure 1.15d. The majority of pyrene-PEG-FITC has been removed in regions with no graphene, but has remained where graphene is present, indicating specific, π -stacking interaction is taking place between the pyrene-PEG-FITC and graphene.

Attachment of GFP-OR nanodiscs to silicon dioxide provides further evidence that the hydrophobic pyrene is weakly bonding to the silicon dioxide surface.

1.6.4. “Coffee-Ring” Effect

When PBASE or pyrene-PEG-NTA were drop-cast onto the device, fluorescence microscope imaging showed that a ring of biomaterial would build up around the outer edge of the droplet. Therefore, in all functionalisation processes the devices were incubated by submerging them in solution rather than dropcasting.

1. Verifying Non-Covalent Functionalisation of Carbon Nanotubes and Graphene

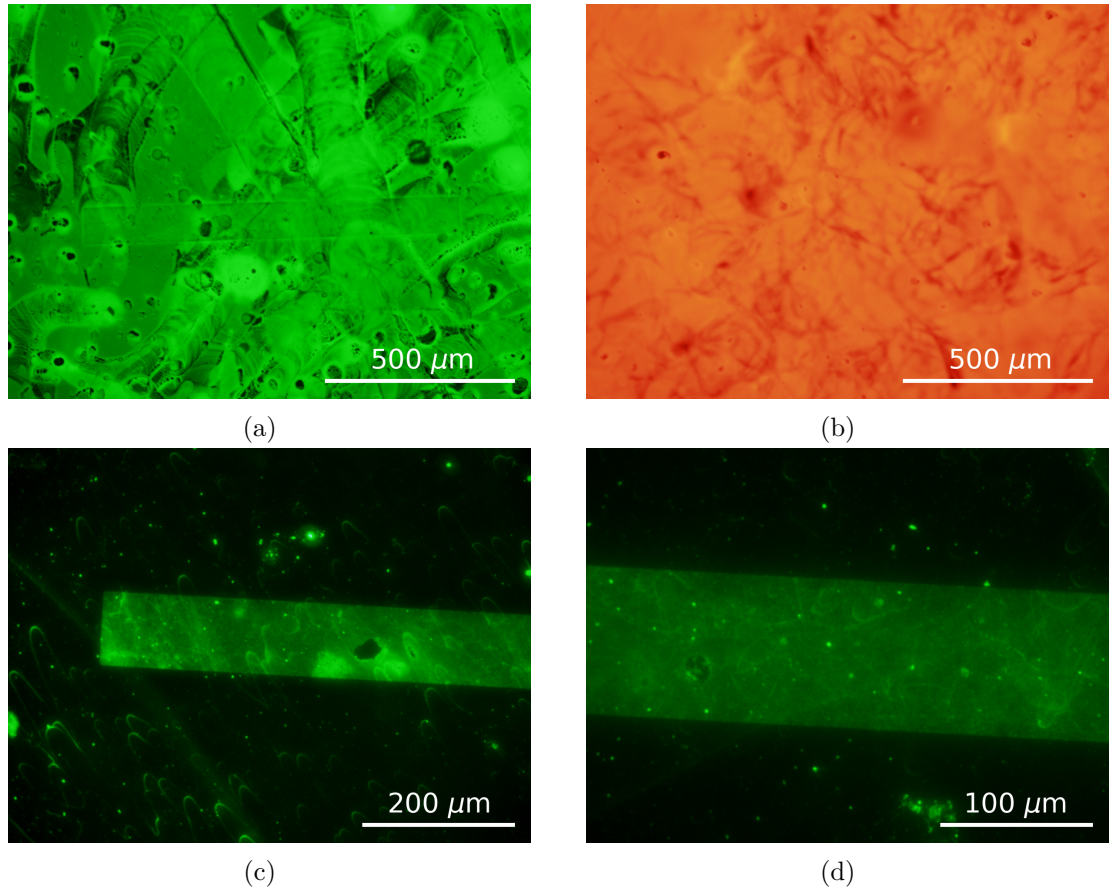


Figure 1.15.: The $1000 \mu\text{m} \times 100 \mu\text{m}$ graphene film in image (a) was functionalised with 1 mM pyrene-PEG-FITC in 1XPBS after oxygen plasma treatment, taken using an FITC filter and a 1.6 s exposure time. (b) shows a silicon dioxide surface which had never been exposed to carbon nanotubes, graphene or photoresist after exposure to 1 mM pyrene-PEG-rhodamine in 1XPBS, taken using a Texas Red filter and a 1.8 s exposure time. Graphene films on a substrate functionalised with 1 mM pyrene-PEG-FITC in 1XPBS after oxygen plasma treatment then cleaned with m-CNT dispersion surfactant (NanoIntegris) are shown in (c) and (d), where a FITC filter was used, with 7.5 s and 7.75 s exposure times respectively.

1.7. Conclusions

After comparing a range of methods for functionalisation of graphene and carbon nanotube networks with odorant receptors, two were identified which showed successful functionalisation of odorant receptors onto transducer devices using appropriate linker molecules. A range of potential obstacles to successful functionalisation were also identified using fluorescence microscopy.

A. Python Code for Data Analysis

A.1. Code Repository

The code used for general analysis of field-effect transistor devices in this thesis was written with Python 3.8.8. Contributors to the code used include Erica Cassie, Erica Happe, Marissa Dierkes and Leo Browning. The code is located on GitHub and the research group OneDrive, and is available on request.

A.2. Atomic Force Microscope Histogram Analysis

The purpose of this code is to analyse atomic force microscope (AFM) images of carbon nanotube networks in .xyz format taken using an atomic force microscope and processed in Gwyddion (see [?@sec-afm-characterisation](#)). It was originally designed by Erica Happe in Matlab, and adapted by Marissa Dierkes and myself for use in Python.

$$f(x) = k_1 \exp\left(-\frac{(x - m_1)^2}{2s_1^2}\right) + k_2 \exp\left(-\frac{(x - m_2)^2}{2s_2^2}\right) + \dots \quad (\text{A.1})$$

The .xyz data is initially sorted into bins with 0.15 nm size. The bin with the maximum number of counts is set at 0 nm, as this peak represents the mean of the surface roughness of the bare silicon. The parameters m_i , s_i , k_i ($i = 1, 2, 3$) are used with objective function Equation A.1 to overlay the data with normal distributions. These fitting parameters represent the mean (m), standard deviation (s) and amplitude (k) of each normal distribution. We can make approximations of some of these fitting parameters using the histogram data.

k_1 is taken to be the maximum y-value of the data being fitted, m_1 is set to zero (used as a point of reference) and s_1 is taken as one-third of the difference between m_1 and the x-value of the first datapoint where the y-value is greater than 1% of k_1 (approximating one standard deviation). We find the distribution given by these values using Equation A.1, and subtract it from the existing dataset.

Then, using the analysis technique outlined by Vobornik *et al.* [84] in Gwyddion, we manually find estimates for the mean m_2 and standard deviation s_2 of the carbon nanotube bundle distribution. We then take k_2 to be the maximum y-value of this modified

A. Python Code for Data Analysis

dataset, and m_1 to be the x-value of the maximum y-value. We then set k_2 so that the height of the resulting distribution at one standard deviation matches the height of the .xyz data histogram. We take this distribution, and subtract it from the existing dataset.

The code also allows for discretely binning continuous data from fitted normal distributions and examining the proportion of counts above or below a particular height. 2.9 nm is roughly where 2 bundles with average size 1.45 nm can start to be present, and is used as an estimate of the boundary value between single-tube bundle diameters and multi-tube bundle diameters.

A.3. Raman Spectroscopy Analysis

The purpose of this code is to analyse a series of Raman spectra taken at different points on a single film (see [?@sec-raman-characterisation](#)).

Data is imported in a tab-delimited text file, and the baseline region between 1400 and 1500 cm⁻¹ is set as zero amplitude for data collected from each film location. The data from each location is then normalised to the D-peak (the maximum point on the D-peak, which lies between 1300 and 1400 cm⁻¹, is set equal to unity). Using these datasets, plots of normalised intensity relative to the D-peak comparing each location can be created. The ratio I^D/I_G can be found by taking the inverse of the maximum point on the G-peak of these normalised plots. A plot of the average intensity across all locations measured can also be created.

A.4. Field-Effect Transistor Analysis

The purpose of this code is to analyse electrical measurements taken of field-effect transistor (FET) devices. Electrical measurements were either taken from the Keysight 4156C Semiconductor Parameter Analyser, National Instruments NI-PXIe or Keysight B1500A Semiconductor Device Analyser as discussed in [?@sec-electrical-characterisation](#); the code is able to analyse data taken from all three measurement setups. The main Python file in the code base consists of three related but independent modules: the first analyses and plots sensing data from the FET devices, the second analyses and plots transfer characteristics from channels across a device, and the third compares individual channel characteristics before and after a modification or after each of several modifications. The code base also features a separate config file and style sheet which govern the behaviour of the main code. The code base was designed collaboratively by myself and Erica Cassie over GitHub using the Sourcetree Git GUI.

The first of the three modules is for processing sensing datasets. This module imports sensing measurements in .csv format and analyses them, then outputs a plot of the

A.4. Field-Effect Transistor Analysis

raw data, alongside multiple plots which have been modified in various ways. It can also fit exponential and linear trendlines to regions of the sensing data, as well as find the signal change per analyte addition, and returns spreadsheets containing the results of these analyses. These spreadsheets include the standard deviation for all included parameters. Modified plots include normalised plots (type of normalisation can be set in config file), plots with fitted curves, plots with the linear baseline drift removed, plots of signal with analyte addition, “despiked” plots and “filtered” plots. It is possible to add annotations to any of these plots using the config file, and it is possible to produce a plot with a combination of these modifications.

The `scipy.optimize.curve_fit` module is used to fit linear and exponential curves to regions of interest of the sensing data. Initial parameters for the `scipy.optimize.curve_fit` module are chosen by approximating fitting parameters in a similar manner to the approach in Section A.2. For a linear fit $mt+b$, the parameters are simply set as $m = 1$ and $b = 0$. For an exponential fit $a \exp(-t/\tau) + c$, c is set as the final current measurement of the region of interest and a is set as the initial current measurement minus c . Then, τ is set as the time where current has dropped to $e^{-1}a + c$.

“Despiked” plots have had spurious datapoints removed through the use of an interquartile range rolling filter. The window size of the rolling filter used was 40 datapoints, and datapoints in each window with a z-score above ± 3 were removed from the plotted/processed data. “Filtered” plots had noise reduced using a moving median filter. The moving median filter is more effective at removing noise than a simple moving average, and has advantages over other filters (such as the Savitzky-Golay filter) when removing noise from data with sharp edges, as is the case for sensing data. Median filtering can also be used for baseline drift compensation, though this approach was not used in this thesis [85]. The moving median filter used had a window of 40 datapoints.

Plots of signal with analyte addition were constructed from current data after first removing baseline drift and applying a moving median filter. A simple difference calculation between the mean of the filtered current before an addition and the mean of the filtered current after the addition was performed at each addition. These differences were then normalised relative to the initial current. The signal with analyte addition give reasonably consistent results regardless of whether baseline drift was removed from the data, as shown in Figure A.1. We can therefore be confident that robust signal with analyte addition plots are robust even in the presence of significant drift.

The second module imports transfer measurements in .csv format and creates combined and individual plots of the eight channels on a single device. In combined plots, channels which are non-working, due to being shorted or non-conducting, are removed via setting a maximum and minimum possible on-current in the config file. Various parameters from the transfer characteristics are saved as a spreadsheet along with standard error. These parameters include on current, off current, subthreshold slope and threshold voltage for the carbon nanotube devices, and on current, off current and major Dirac point voltage for graphene devices. The device type being analysed can be set in the config file.

A. Python Code for Data Analysis

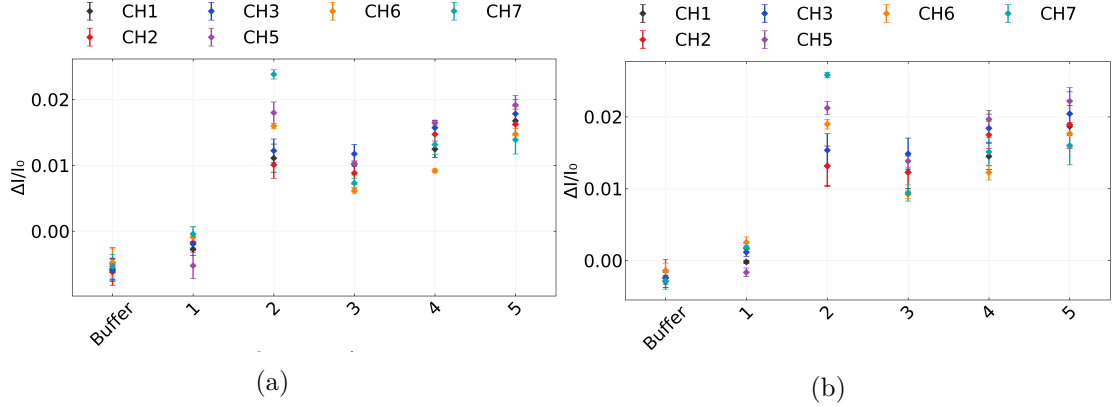


Figure A.1.: A comparison of signal with analyte addition plots taken from the same salt concentration sensing dataset (the same dataset as used in [?@fig-salt-conc-sensing](#)). In (a), a simple difference calculation performed on filtered data was used, while in (b) the same calculation was performed on filtered data with the baseline drift removed, the method used in the body of the thesis.

The third module imports several transfer measurements in .csv format and allows for comparison of the same channel before and after some modification. It also calculates the shift in either threshold voltage or major Dirac voltage of the device.

B. Vapour Delivery System

B.1. Technical Notes

Two LabView Virtual Instruments (VIs) were adapted from pre-existing VIs for operating the mass flow controllers and monitoring vapour flow into the device chamber, as well as monitoring temperature and humidity in the vapour delivery system's manifold. These VIs were named “ ” A third VI was developed in parallel which combined the first two Virtual Instruments, alongside allowing the sequence of values to control the mass flow controllers.

From Honours report: “ ” Figure 12 gives the right side of the front panel of the LabView VI sample with `vapour.VI`, which lets us preset an autonomously-performed vapour sensing sequence. Each row in each array module corresponds to a different step in this sequence. The ‘`howManySteps`’ module lets us set how many of these steps are performed. The ‘`Durations Array`’ module determines the length of time in seconds each step is performed over. The ‘`Carrier Flows Array`’ and ‘`Dilution Flows Array`’ modules let us set the carrier flow and dilution flow, respectively, in standard cubic centimetres per minute (sccm) through the gas rig at each step. The carrier flow pushes analyte vapour into the vapour-sensing device chamber, while dilution flow is used to modify the flow behaviour of the analyte vapour entering the chamber. The vapour sensing sequence as depicted in Figure 12 was used for all vapour sensing runs in this investigation. At the end of the sequence, the data collected about the vapour sensing process was saved as an `.lvm` file. “ ”

B.2. Future Improvements

Bibliography

- [1] Brenda Long, Mary Manning, Micheal Burke, et al. “Non-Covalent Functionalization of Graphene Using Self-Assembly of Alkane-Amines”. In: *Advanced Functional Materials* 22.4 (Feb. 2012), pp. 717–725. ISSN: 1616-3028. DOI: 10.1002/adfm.201101956. URL: <https://onlinelibrary.wiley.com/doi/full/10.1002/adfm.201101956>.
- [2] Antonello Di Crescenzo, Valeria Ettorre, and Antonella Fontana. “Non-covalent and reversible functionalization of carbon nanotubes”. In: *Beilstein Journal of Nanotechnology* 5.1 (2014), p. 1675. ISSN: 21904286. DOI: 10.3762/BJNANO.5.178. URL: [/pmc/articles/PMC4222398/](https://pmc/articles/PMC4222398/)?report=abstract%20https://www.ncbi.nlm.nih.gov/pmc/articles/PMC4222398/.
- [3] Shiyu Wang, Md Zakir Hossain, Kazuo Shinozuka, et al. “Graphene field-effect transistor biosensor for detection of biotin with ultrahigh sensitivity and specificity”. In: *Biosensors and Bioelectronics* 165 (Oct. 2020), p. 112363. ISSN: 18734235. DOI: 10.1016/j.bios.2020.112363. URL: [/pmc/articles/PMC7272179/](https://pmc/articles/PMC7272179/)?report=abstract%20https://www.ncbi.nlm.nih.gov/pmc/articles/PMC7272179/.
- [4] Vladyslav Mishyn, Adrien Hugo, Teresa Rodrigues, et al. “The holy grail of pyrene-based surface ligands on the sensitivity of graphene-based field effect transistors”. In: *Sensors and Diagnostics* 1.2 (Mar. 2022), pp. 235–244. ISSN: 2635-0998. DOI: 10.1039/D1SD00036E. URL: <https://pubs.rsc.org/en/content/articlehtml/2022/sd/d1sd00036e>%20https://pubs.rsc.org/en/content/articlelanding/2022/sd/d1sd00036e.
- [5] Mitchell B. Lerner, Felipe Matsunaga, Gang Hee Han, et al. “Scalable production of highly sensitive nanosensors based on graphene functionalized with a designed G protein-coupled receptor”. In: *Nano Letters* 14.5 (May 2014), pp. 2709–2714. ISSN: 15306992. DOI: 10.1021/NL5006349/SUPPL_FILE/NL5006349_SI_001.PDF. URL: <https://pubs.acs.org/doi/full/10.1021/nl5006349>.
- [6] Kishan Thodkar, Pierre Andre Cazade, Frank Bergmann, et al. “Self-assembled pyrene stacks and peptide monolayers tune the electronic properties of functionalized electrolyte-gated graphene field-effect transistors”. In: *ACS Applied Materials and Interfaces* 13.7 (Feb. 2021), pp. 9134–9142. ISSN: 19448252. DOI: 10.1021/ACSAM.0C18485/ASSET/IMAGES/LARGE/AM0C18485_0006.jpeg. URL: <https://pubs.acs.org/doi/full/10.1021/acsami.0c18485>.

Bibliography

- [7] Carbonnanotube. *File:Noncovalent carboncarbonnanotube.png*. 2015. URL: https://en.m.wikipedia.org/wiki/File:Noncovalent_carboncarbonnanotube.png (visited on 2023-10-13).
- [8] Emilio M. Pérez and Nazario Martín. “ $\pi-\pi$ interactions in carbon nanostructures”. In: *Chemical Society Reviews* 44.18 (Sept. 2015), pp. 6425–6433. ISSN: 1460-4744. DOI: 10.1039/C5CS00578G. URL: <https://pubs.rsc.org/en/content/articlehtml/2015/cs/c5cs00578g%20https://pubs.rsc.org/en/content/articlelanding/2015/cs/c5cs00578g>.
- [9] Chelsea R. Martinez and Brent L. Iverson. “Rethinking the term “pi-stacking””. In: *Chemical Science* 3.7 (June 2012), pp. 2191–2201. ISSN: 2041-6539. DOI: 10.1039/C2SC20045G. URL: <https://pubs.rsc.org/en/content/articlehtml/2012/sc/c2sc20045g%20https://pubs.rsc.org/en/content/articlelanding/2012/sc/c2sc20045g>.
- [10] Greg T. Hermanson. “Buckyballs, Fullerenes, and Carbon Nanotubes”. In: *Bioconjugate Techniques* (Jan. 2013), pp. 741–755. DOI: 10.1016/B978-0-12-382239-0.00016-9.
- [11] Yan Zhou, Yi Fang, and Ramaraja P. Ramasamy. “Non-Covalent Functionalization of Carbon Nanotubes for Electrochemical Biosensor Development”. In: *Sensors (Basel, Switzerland)* 19.2 (Jan. 2019). ISSN: 1424-8220. DOI: 10.3390/S19020392. URL: <https://pubmed.ncbi.nlm.nih.gov/30669367/>.
- [12] J. A. M. J. Frisch and G. W. Trucks and H. B. Schlegel and G. E. Scuseria and M. A. Robb and J. R. Cheeseman and G. Scalmani and V. Barone and G. A. Petersson and H. Nakatsuji and X. Li and M. Caricato and A. V. Marenich and J. Bloino and B. G. Janesko and R. G, J. E. Peralta, F. Ogliaro, et al. *Gaussian~16 Revision C.01*. 2016.
- [13] Yasuhiro Oishi, Hirotsugu Ogi, Satoshi Hagiwara, et al. “Theoretical Analysis on the Stability of 1-Pyrenebutanoic Acid Succinimidyl Ester Adsorbed on Graphene”. In: *ACS Omega* 7.35 (Sept. 2022), pp. 31120–31125. ISSN: 24701343. DOI: 10.1021/AC SOMEWA.2C03257 / ASSET / IMAGES / LARGE / AO2C03257_0004.JPEG. URL: <https://pubs.acs.org/doi/full/10.1021/acsomega.2c03257>.
- [14] R. J. Chen, Y. Zhang, D. Wang, et al. “Noncovalent sidewall functionalization of single-walled carbon nanotubes for protein immobilization”. In: *Journal of the American Chemical Society* 123.16 (2001), pp. 3838–3839. ISSN: 00027863. DOI: 10.1021/ja010172b. URL: <http://pubs.acs.org..>
- [15] Greg T. Hermanson. “The Reactions of Bioconjugation”. In: *Bioconjugate Techniques* (Jan. 2013), pp. 229–258. DOI: 10.1016/B978-0-12-382239-0.00003-0.
- [16] Kenzo Maehashi, Taiji Katsura, Kagan Kerman, et al. “Label-free protein biosensor based on aptamer-modified carbon nanotube field-effect transistors”. In: *Analytical Chemistry* 79.2 (Jan. 2007), pp. 782–787. ISSN: 00032700. DOI: 10.1021/ac060830g. URL: <https://pubs.acs.org/doi/full/10.1021/ac060830g>.

- [17] Cristina García-Aljaro, Lakshmi N. Cella, Dhamanand J. Shirale, et al. “Carbon nanotubes-based chemiresistive biosensors for detection of microorganisms”. In: *Biosensors and Bioelectronics* 26.4 (Dec. 2010), pp. 1437–1441. ISSN: 09565663. DOI: 10.1016/j.bios.2010.07.077.
- [18] Lakshmi N. Cella, Pablo Sanchez, Wenwan Zhong, et al. “Nano aptasensor for Protective Antigen Toxin of Anthrax”. In: *Analytical Chemistry* 82.5 (Mar. 2010), pp. 2042–2047. ISSN: 00032700. DOI: 10.1021/ac902791q. URL: <https://pubs.acs.org/doi/full/10.1021/ac902791q>.
- [19] Basanta K. Das, Chaker Tlili, Sushmee Badhulika, et al. “Single-walled carbon nanotubes chemiresistor aptasensors for small molecules: Picomolar level detection of adenosine triphosphate”. In: *Chemical Communications* 47.13 (Mar. 2011), pp. 3793–3795. ISSN: 1364548X. DOI: 10.1039/c0cc04733c. URL: <https://pubs.rsc.org/en/content/articlehtml/2011/cc/c0cc04733c%20https://pubs.rsc.org/en/content/articlelanding/2011/cc/c0cc04733c>.
- [20] Koen Besteman, Jeong O. Lee, Frank G.M. Wiertz, et al. “Enzyme-coated carbon nanotubes as single-molecule biosensors”. In: *Nano Letters* 3.6 (June 2003), pp. 727–730. ISSN: 15306984. DOI: 10.1021/NL034139U / ASSET / IMAGES / LARGE/NL034139UF00004.JPG. URL: <https://pubs.acs.org/doi/full/10.1021/nl034139u>.
- [21] Deana Kwong Hong Tsang, Tyler J. Lieberthal, Clare Watts, et al. “Chemically Functionalised Graphene FET Biosensor for the Label-free Sensing of Exosomes”. In: *Scientific Reports* 9.1 (Sept. 2019), pp. 1–10. ISSN: 20452322. DOI: 10.1038/s41598-019-50412-9. URL: <https://www.nature.com/articles/s41598-019-50412-9>.
- [22] Gregory R. Wiedman, Yanan Zhao, Arkady Mustaev, et al. “An Aptamer-Based Biosensor for the Azole Class of Antifungal Drugs”. In: *mSphere* 2.4 (Aug. 2017). ISSN: 23795042. DOI: 10.1128/msphere.00274-17. URL: <https://pmc.ncbi.nlm.nih.gov/pmc/articles/PMC5566834/>.
- [23] Zhaoli Gao, Han Xia, Jonathan Zauberman, et al. “Detection of Sub-fM DNA with Target Recycling and Self-Assembly Amplification on Graphene Field-Effect Biosensors”. In: *Nano Letters* 18.6 (June 2018), pp. 3509–3515. ISSN: 15306992. DOI: 10.1021/acs.nanolett.8b00572. URL: <https://pubs.acs.org/doi/full/10.1021/acs.nanolett.8b00572>.
- [24] Nikita Nekrasov, Natalya Yakunina, Averyan V. Pushkarev, et al. “Spectral-phase interferometry detection of ochratoxin a via aptamer-functionalized graphene coated glass”. In: *Nanomaterials* 11.1 (Jan. 2021), pp. 1–10. ISSN: 20794991. DOI: 10.3390/nano11010226. URL: <https://www.mdpi.com/2079-4991/11/1/226>.

Bibliography

- [25] Michael T. Hwang, B. Landon Preston, Lee Joon, et al. "Highly specific SNP detection using 2D graphene electronics and DNA strand displacement". In: *Proceedings of the National Academy of Sciences of the United States of America* 113.26 (June 2016), pp. 7088–7093. ISSN: 10916490. DOI: 10.1073/pnas.1603753113. URL: <https://www.pnas.org/doi/abs/10.1073/pnas.1603753113>.
- [26] Zhuang Hao, Yunlu Pan, Cong Huang, et al. "Modulating the Linker Immobilization Density on Aptameric Graphene Field Effect Transistors Using an Electric Field". In: *ACS Sensors* 5.8 (Aug. 2020), pp. 2503–2513. ISSN: 23793694. DOI: 10.1021/ACSSENSORS.0C00752/ASSET/IMAGES/LARGE/SE0C00752_0008. JPEG. URL: <https://pubs.acs.org/doi/full/10.1021/acssensors.0c00752>.
- [27] Mohd Maidin Nur Nasyifa, A. Rahim Ruslinda, Nur Hamidah Abdul Halim, et al. "Immuno-probed graphene nanoplatelets on electrolyte-gated field-effect transistor for stable cortisol quantification in serum". In: *Journal of the Taiwan Institute of Chemical Engineers* 117 (Dec. 2020), pp. 10–18. ISSN: 18761070. DOI: 10.1016/j.jtice.2020.12.008.
- [28] Rui Campos, Jérôme Borme, Joana Rafaela Guerreiro, et al. "Attomolar label-free detection of dna hybridization with electrolyte-gated graphene field-effect transistors". In: *ACS Sensors* 4.2 (Feb. 2019), pp. 286–293. ISSN: 23793694. DOI: 10.1021/acssensors.8b00344. URL: <https://pubs.acs.org/doi/full/10.1021/acssensors.8b00344>.
- [29] Murat Kuscu, Hamideh Ramezani, Ergin Dinc, et al. "Graphene-based Nanoscale Molecular Communication Receiver: Fabrication and Microfluidic Analysis". In: (June 2020). arXiv: 2006.15470. URL: <https://arxiv.org/abs/2006.15470v2>.
- [30] Shicai Xu, Jian Zhan, Baoyuan Man, et al. "Real-time reliable determination of binding kinetics of DNA hybridization using a multi-channel graphene biosensor". In: *Nature Communications* 8.1 (Mar. 2017), pp. 1–10. ISSN: 20411723. DOI: 10.1038/ncomms14902. URL: <https://www.nature.com/articles/ncomms14902>.
- [31] Niazul I. Khan, Mohammad Mousazadehkasin, Sujoy Ghosh, et al. "An integrated microfluidic platform for selective and real-time detection of thrombin biomarkers using a graphene FET". In: *Analyst* 145.13 (June 2020), pp. 4494–4503. ISSN: 13645528. DOI: 10.1039/d0an00251h. URL: <https://pubs.rsc.org/en/content/articlehtml/2020/an/d0an00251h%20https://pubs.rsc.org/en/content/articlelanding/2020/an/d0an00251h>.
- [32] T Ono, K Kamada, R Hayashi, et al. "Lab-on-a-graphene-FET detection of key molecular events underpinning influenza 2 virus infection and effect of antiviral drugs 3 Running title: Graphene-FET detects reactions in an influenza infection MAIN TEXT". In: *bioRxiv* (Mar. 2020), p. 2020.03.18.996884. DOI: 10.1101/2020.03.18.996884. URL: <https://doi.org/10.1101/2020.03.18.996884>.

- [33] Han Yue Zheng, Omar A. Alsager, Bicheng Zhu, et al. “Electrostatic gating in carbon nanotube aptasensors”. In: *Nanoscale* 8.28 (July 2016), pp. 13659–13668. ISSN: 20403372. DOI: 10.1039/c5nr08117c. URL: <https://pubs.rsc.org/en/content/articlehtml/2016/nr/c5nr08117c%20https://pubs.rsc.org/en/content/articlelanding/2016/nr/c5nr08117c>.
- [34] Jun Pyo Kim, Byung Yang Lee, Joohyung Lee, et al. “Enhancement of sensitivity and specificity by surface modification of carbon nanotubes in diagnosis of prostate cancer based on carbon nanotube field effect transistors”. In: *Biosensors and Bioelectronics* 24.11 (July 2009), pp. 3372–3378. ISSN: 09565663. DOI: 10.1016/j.bios.2009.04.048. URL: <https://pubmed.ncbi.nlm.nih.gov/19481922/>.
- [35] Jin Yoo, Daesan Kim, Heehong Yang, et al. “Olfactory receptor-based CNT-FET sensor for the detection of DMMP as a simulant of sarin”. In: *Sensors and Actuators B: Chemical* 354 (Mar. 2022), p. 131188. ISSN: 0925-4005. DOI: 10.1016/J.SNB.2021.131188.
- [36] Jagriti Sethi, Michiel Van Bulck, Ahmed Suhail, et al. “A label-free biosensor based on graphene and reduced graphene oxide dual-layer for electrochemical determination of beta-amyloid biomarkers”. In: *Microchimica Acta* 187.5 (May 2020), pp. 1–10. ISSN: 14365073. DOI: 10.1007/s00604-020-04267-x. URL: <https://link.springer.com/article/10.1007/s00604-020-04267-x>.
- [37] Yasuhide Ohno, Kenzo Maehashi, and Kazuhiko Matsumoto. “Label-free biosensors based on aptamer-modified graphene field-effect transistors”. In: *Journal of the American Chemical Society* 132.51 (Dec. 2010), pp. 18012–18013. ISSN: 00027863. DOI: 10.1021/ja108127r. URL: <https://pubs.acs.org/doi/full/10.1021/ja108127r>.
- [38] Ryan J. Lopez, Sofia Babanova, Kateryna Artyushkova, et al. “Surface modifications for enhanced enzyme immobilization and improved electron transfer of PQQ-dependent glucose dehydrogenase anodes”. In: *Bioelectrochemistry* 105 (Oct. 2015), pp. 78–87. ISSN: 1878562X. DOI: 10.1016/j.bioelechem.2015.05.010. URL: <https://pubmed.ncbi.nlm.nih.gov/26011132/>.
- [39] Guinevere Strack, Robert Nichols, Plamen Atanassov, et al. “Modification of carbon nanotube electrodes with 1-pyrenebutanoic acid, succinimidyl ester for enhanced bioelectrocatalysis”. In: *Methods in Molecular Biology* 1051 (2013), pp. 217–228. ISSN: 10643745. DOI: 10.1007/978-1-62703-550-7_14. URL: <https://pubmed.ncbi.nlm.nih.gov/23934807/>.
- [40] Malkom Hinnemo, Jie Zhao, Patrik Ahlberg, et al. “On Monolayer Formation of Pyrenebutyric Acid on Graphene”. In: *Langmuir* 33.15 (Apr. 2017), pp. 3588–3593. ISSN: 15205827. DOI: 10.1021/ACS.LANGMUIR.6B04237/ASSET/IMAGES/LARGE/LA-2016-04237V_0003.JPG. URL: <https://pubs.acs.org/doi/full/10.1021/acs.langmuir.6b04237>.

Bibliography

- [41] Xue V. Zhen, Emily G. Swanson, Justin T. Nelson, et al. “Noncovalent monolayer modification of graphene using pyrene and cyclodextrin receptors for chemical sensing”. In: *ACS Applied Nano Materials* 1.6 (June 2018), pp. 2718–2726. ISSN: 25740970. DOI: 10.1021/ACSANM.8B00420/ASSET/IMAGES/LARGE/AN-2018-00420J_0004.jpeg. URL: <https://pubs.acs.org/doi/full/10.1021/acsanm.8b00420>.
- [42] Ryan J. White, Noelle Phares, Arica A. Lubin, et al. “Optimization of electrochemical aptamer-based sensors via optimization of probe packing density and surface chemistry”. In: *Langmuir : the ACS journal of surfaces and colloids* 24.18 (Sept. 2008), pp. 10513–10518. ISSN: 0743-7463. DOI: 10.1021/LA800801V. URL: <https://pubmed.ncbi.nlm.nih.gov/18690727/>.
- [43] Yu Chen, Tze Sian Pui, Patthara Kongsuphol, et al. “Aptamer-based array electrodes for quantitative interferon- γ detection”. In: *Biosensors and Bioelectronics* 53 (Mar. 2014), pp. 257–262. ISSN: 1873-4235. DOI: 10.1016/J.BIOS.2013.09.046. URL: <https://pubmed.ncbi.nlm.nih.gov/24144556/>.
- [44] Greg T. Hermanson. “Homobifunctional Crosslinkers”. In: *Bioconjugate Techniques* (Jan. 2013), pp. 275–298. DOI: 10.1016/B978-0-12-382239-0.00005-4.
- [45] *1-Pyrenebutyric acid N-hydroxysuccinimide ester - [1H NMR] - Spectrum - SpectraBase*. URL: <https://spectrabase.com/spectrum/FxRoJanrm9t> (visited on 2023-10-19).
- [46] R. G. Lebel and D. A.I. Goring. “Density, Viscosity, Refractive Index, and Hygroscopicity of Mixtures of Water and Dimethyl Sulfoxide”. In: *Journal of Chemical and Engineering Data* 7.1 (Jan. 1962), pp. 100–101. ISSN: 15205134. DOI: 10.1021/JE60012A032/ASSET/JE60012A032.FP.PNG_V03. URL: <https://pubs.acs.org/doi/abs/10.1021/je60012a032>.
- [47] Alexander B. Artyukhin, Michael Stadermann, Raymond W. Friddle, et al. “Controlled electrostatic gating of carbon nanotube FET devices”. In: *Nano Letters* 6.9 (Sept. 2006), pp. 2080–2085. ISSN: 15306984. DOI: 10.1021/NL061343J/SUPPLFILE/NL061343JSI20060609_104449.PDF. URL: <https://pubs.acs.org/doi/full/10.1021/nl061343j>.
- [48] Iddo Heller, Anne M. Janssens, Jaan Männik, et al. “Identifying the mechanism of biosensing with carbon nanotube transistors”. In: *Nano Letters* 8.2 (Feb. 2008), pp. 591–595. ISSN: 15306984. DOI: 10.1021/NL072996I/SUPPL_FILE/NL072996ISI20071116_124235.PDF. URL: <https://pubs.acs.org/doi/full/10.1021/nl072996i>.
- [49] Thanihaichelvan Murugathas, Han Yue Zheng, Damon Colbert, et al. “Biosensing with Insect Odorant Receptor Nanodiscs and Carbon Nanotube Field-Effect Transistors”. In: *ACS Applied Materials and Interfaces* 11.9 (Mar. 2019), pp. 9530–9538. ISSN: 19448252. DOI: 10.1021/ACSAMI.8B19433/ASSET/IMAGES/LARGE/AM-2018-19433U_0002.jpeg. URL: <https://pubs.acs.org/doi/full/10.1021/acsami.8b19433>.

- [50] M. Mohsen-Nia, H. Amiri, and B. Jazi. "Dielectric constants of water, methanol, ethanol, butanol and acetone: Measurement and computational study". In: *Journal of Solution Chemistry* 39.5 (2010), pp. 701–708. ISSN: 00959782. DOI: 10.1007/S10953-010-9538-5.
- [51] Johannes Hunger, Richard Buchner, Mohamed E. Kandil, et al. "Relative permittivity of dimethylsulfoxide and N, N -dimethylformamide at temperatures from (278 to 328) K and pressures from (0.1 to 5) MPa". In: *Journal of Chemical and Engineering Data* 55.5 (May 2010), pp. 2055–2065. ISSN: 00219568. DOI: 10.1021/JE9010773 / SUPPL _FILE / JE9010773 _SI _001.PDF. URL: <https://pubs.acs.org/doi/full/10.1021/je9010773>.
- [52] Bajramshahe Shkodra, Mattia Petrelli, Martina Aurora Costa Angeli, et al. "Electrolyte-gated carbon nanotube field-effect transistor-based biosensors: Principles and applications". In: *Applied Physics Reviews* 8.4 (Dec. 2021), p. 41325. ISSN: 19319401. DOI: 10.1063 / 5 . 0058591 / 1076095. URL: [/aip/apr/article/8/4/041325/1076095/Electrolyte-gated-carbon-nanotube-field-effect](https://aip/apr/article/8/4/041325/1076095/Electrolyte-gated-carbon-nanotube-field-effect).
- [53] Ning Gao, Teng Gao, Xiao Yang, et al. "Specific detection of biomolecules in physiological solutions using graphene transistor biosensors". In: *Proceedings of the National Academy of Sciences of the United States of America* 113.51 (Dec. 2016), pp. 14633–14638. ISSN: 10916490. DOI: 10.1073/PNAS.1625010114 / SUPPL _FILE / PNAS.201625010SI.PDF. URL: <https://www.pnas.org/doi/abs/10.1073/pnas.1625010114>.
- [54] Kyoungseon Min, Jungbae Kim, Kyungmoon Park, et al. "Enzyme immobilization on carbon nanomaterials: Loading density investigation and zeta potential analysis". In: *Journal of Molecular Catalysis B: Enzymatic* 83 (Nov. 2012), pp. 87–93. ISSN: 1381-1177. DOI: 10.1016/J.MOLCATB.2012.07.009.
- [55] Mercè Pacios, Iñigo Martin-Fernandez, Xavier Borrisé, et al. "Real time protein recognition in a liquid-gated carbon nanotube field-effect transistor modified with aptamers". In: *Nanoscale* 4.19 (Sept. 2012), pp. 5917–5923. ISSN: 2040-3372. DOI: 10.1039/C2NR31257C. URL: <https://pubs.rsc.org/en/content/articlehtml/2012/nr/c2nr31257c%20https://pubs.rsc.org/en/content/articlelanding/2012/nr/c2nr31257c>.
- [56] Marcin S. Filipiak, Marcel Rother, Nesha M. Andoy, et al. "Highly sensitive, selective and label-free protein detection in physiological solutions using carbon nanotube transistors with nanobody receptors". In: *Sensors and Actuators B: Chemical* 255 (Feb. 2018), pp. 1507–1516. ISSN: 0925-4005. DOI: 10.1016/J.SNB.2017.08.164.
- [57] Jing Tong, Lei Zhang, Yi Wang, et al. "High response photodetection by applying the optimized photoreceptor protein modification on graphene based field effect transistors". In: *FrMat* 7 (July 2020), p. 222. ISSN: 22968016. DOI: 10.3389 / FMATS.2020.00222. URL: <https://ui.adsabs.harvard.edu/abs/2020FrMat...7..222T/abstract>.

Bibliography

- [58] Jie Liu, Florence Appaix, Olivier Bibari, et al. “Control of neuronal network organization by chemical surface functionalization of multi-walled carbon nanotube arrays”. In: *Nanotechnology* 22.19 (May 2011). ISSN: 1361-6528. DOI: 10.1088/0957-4484/22/19/195101. URL: <https://pubmed.ncbi.nlm.nih.gov/21436508/>.
- [59] Christoph Fenzl, Pranati Nayak, Thomas Hirsch, et al. “Laser-Scribed Graphene Electrodes for Aptamer-Based Biosensing”. In: *ACS sensors* 2.5 (May 2017), pp. 616–620. ISSN: 2379-3694. DOI: 10.1021/ACSSENSORS.7B00066. URL: <https://pubmed.ncbi.nlm.nih.gov/28723173/>.
- [60] Deepak Sehgal and Inder K. Vijay. “A Method for the High Efficiency of Water-Soluble Carbodiimide-Mediated Amidation”. In: *Analytical Biochemistry* 218.1 (Apr. 1994), pp. 87–91. ISSN: 0003-2697. DOI: 10.1006/ABIO.1994.1144.
- [61] Greg T. Hermanson. “Zero-Length Crosslinkers”. In: *Bioconjugate Techniques* (Jan. 2013), pp. 259–273. DOI: 10.1016/B978-0-12-382239-0.00004-2.
- [62] Greg T. Hermanson. “Microparticles and Nanoparticles”. In: *Bioconjugate Techniques* (Jan. 2013), pp. 549–587. DOI: 10.1016/B978-0-12-382239-0.00014-5.
- [63] Gang Wei, Changjiang Pan, Jörg Reichert, et al. “Controlled assembly of protein-protected gold nanoparticles on noncovalent functionalized carbon nanotubes”. In: *Carbon* 48.3 (Mar. 2010), pp. 645–653. ISSN: 0008-6223. DOI: 10.1016/J.CARBON.2009.10.006.
- [64] Meng Lan, Guoli Fan, Wei Sun, et al. “Synthesis of hybrid Zn–Al–In mixed metal oxides/carbon nanotubes composite and enhanced visible-light-induced photocatalytic performance”. In: *Applied Surface Science* 282 (Oct. 2013), pp. 937–946. ISSN: 0169-4332. DOI: 10.1016/J.APSUSC.2013.06.095.
- [65] Mitchell B. Lerner, James M. Resczenski, Akshay Amin, et al. “Toward quantifying the electrostatic transduction mechanism in carbon nanotube molecular sensors”. In: *Journal of the American Chemical Society* 134.35 (Sept. 2012), pp. 14318–14321. ISSN: 00027863. DOI: 10.1021/JA306363V/SUPPL_FILE/JA306363V_SI_001.PDF. URL: <https://pubs.acs.org/doi/full/10.1021/ja306363v>.
- [66] Michael Holzinger, Jessica Baur, Raoudha Haddad, et al. “Multiple functionalization of single-walled carbon nanotubes by dip coating”. In: *Chemical Communications* 47.8 (Feb. 2011), pp. 2450–2452. ISSN: 1364-548X. DOI: 10.1039/C0CC03928D. URL: <https://pubs.rsc.org/en/content/articlehtml/2011/cc/c0cc03928d%20https://pubs.rsc.org/en/content/articlelanding/2011/cc/c0cc03928d>.
- [67] Yoshihisa Amano, Ayako Koto, Shohei Matsuzaki, et al. “Construction of a biointerface on a carbon nanotube surface for efficient electron transfer”. In: *Materials Letters* 174 (July 2016), pp. 184–187. ISSN: 0167-577X. DOI: 10.1016/J.MATLET.2016.03.113.

- [68] Y. Y. Chang, H. Li, and H. Sun. “Immobilized Metal Affinity Chromatography (IMAC) for Metalloproteomics and Phosphoproteomics”. In: *Inorganic and Organometallic Transition Metal Complexes with Biological Molecules and Living Cells* (Jan. 2017), pp. 329–353. DOI: 10.1016/B978-0-12-803814-7.00009-5.
- [69] Brett R. Goldsmith, Joseph J. Mitala, Jesusa Josue, et al. “Biomimetic chemical sensors using nanoelectronic readout of olfactory receptor proteins”. In: *ACS Nano* 5.7 (July 2011), pp. 5408–5416. ISSN: 19360851. DOI: 10.1021/NN200489J/_SUPPL_FILE/NN200489J_SI_001.PDF. URL: <https://pubs.acs.org/doi/full/10.1021/nn200489j>.
- [70] Alexander Star, Jean Christophe P. Gabriel, Keith Bradley, et al. “Electronic detection of specific protein binding using nanotube FET devices”. In: *Nano Letters* 3.4 (Apr. 2003), pp. 459–463. ISSN: 15306984. DOI: 10.1021/NL0340172/_SUPPL_FILE/NL0340172SI20030213_114154.PDF. URL: <https://pubs.acs.org/doi/full/10.1021/nl0340172>.
- [71] Christopher M. Dundas, Daniel Demonte, and Sheldon Park. “Streptavidin-biotin technology: Improvements and innovations in chemical and biological applications”. In: *Applied Microbiology and Biotechnology* 97.21 (Nov. 2013), pp. 9343–9353. ISSN: 01757598. DOI: 10.1007/S00253-013-5232-Z/_FIGURES/3. URL: <https://link.springer.com/article/10.1007/s00253-013-5232-z>.
- [72] Greg T. Hermanson. “(Strept)avidin–Biotin Systems”. In: *Bioconjugate Techniques* (Jan. 2013), pp. 465–505. DOI: 10.1016/B978-0-12-382239-0.00011-X.
- [73] Michael Fairhead and Mark Howarth. “Site-specific biotinylation of purified proteins using BirA”. In: *Methods in molecular biology (Clifton, N.J.)* 1266 (2015), p. 171. ISSN: 10643745. DOI: 10.1007/978-1-4939-2272-7_12. URL: /pmc/articles/PMC4304673/_20/_pmc/_articles/_PMC4304673/_?report=abstract%20<https://www.ncbi.nlm.nih.gov/pmc/articles/PMC4304673/>.
- [74] Greg T. Hermanson. “PEGylation and Synthetic Polymer Modification”. In: *Bioconjugate Techniques* (Jan. 2013), pp. 787–838. DOI: 10.1016/B978-0-12-382239-0.00018-2.
- [75] Mehdi Meran, Pelin Deniz Akkus, Ozge Kurkcuoglu, et al. “Noncovalent Pyrene-Polyethylene Glycol Coatings of Carbon Nanotubes Achieve in Vitro Biocompatibility”. In: *Langmuir* 34.40 (Oct. 2018), pp. 12071–12082. ISSN: 15205827. DOI: 10.1021/ACS.LANGMUIR.8B00971. URL: <https://pubs.acs.org/doi/full/10.1021/acs.langmuir.8b00971>.
- [76] Hiroko Miki, Atsunobu Isobayashi, Tatsuro Saito, et al. “Ionic liquids with wafer-scalable graphene sensors for biological detection”. In: *IEEE Transactions on Nanobioscience* 18.2 (Apr. 2019), pp. 216–219. ISSN: 15361241. DOI: 10.1109/TNB.2019.2905286.

Bibliography

- [77] Zhenghai Tang, Yanda Lei, Baochun Guo, et al. “The use of rhodamine B-decorated graphene as a reinforcement in polyvinyl alcohol composites”. In: *Polymer* 53.2 (Jan. 2012), pp. 673–680. ISSN: 0032-3861. DOI: 10.1016/J.POLYMER.2011.11.056.
- [78] Sumedh P. Surwade, Sergei N. Smirnov, Ivan V. Vlassiouk, et al. “Water desalination using nanoporous single-layer graphene”. In: *Nature Nanotechnology* 2015 10:5 10.5 (Mar. 2015), pp. 459–464. ISSN: 1748-3395. DOI: 10.1038/nano.2015.37. URL: <https://www.nature.com/articles/nano.2015.37>.
- [79] Ali Ashraf, Yanbin Wu, Michael C. Wang, et al. “Spectroscopic investigation of the wettability of multilayer graphene using highly ordered pyrolytic graphite as a model material”. In: *Langmuir* 30.43 (Nov. 2014), pp. 12827–12836. ISSN: 15205827. DOI: 10.1021/LA503089K/SUPPL_FILE/LA503089K_SI_001.PDF. URL: <https://pubs.acs.org/doi/full/10.1021/la503089k>.
- [80] Grzegorz Stando, Damian Łukawski, Filip Lisiecki, et al. “Intrinsic hydrophilic character of carbon nanotube networks”. In: *Applied Surface Science* 463 (Jan. 2019), pp. 227–233. ISSN: 0169-4332. DOI: 10.1016/J.APSUSC.2018.08.206.
- [81] Young Jun Shin, Yingying Wang, Han Huang, et al. “Surface-energy engineering of graphene”. In: *Langmuir* 26.6 (Mar. 2010), pp. 3798–3802. ISSN: 07437463. DOI: 10.1021/LA100231U/ASSET/IMAGES/LARGE/LA-2010-00231U_0005.JPG. URL: <https://pubs.acs.org/doi/full/10.1021/la100231u>.
- [82] Jeng Hao Pai, Yuli Wang, Gina To A. Salazar, et al. “A Photoresist with Low Fluorescence for Bioanalytical Applications”. In: *Analytical chemistry* 79.22 (Nov. 2007), p. 8774. ISSN: 00032700. DOI: 10.1021/AC071528Q. URL: /pmc/articles/PMC2435225/%20/pmc/articles/PMC2435225/?report=abstract%20https://www.ncbi.nlm.nih.gov/pmc/articles/PMC2435225/.
- [83] Creative PEGWorks. *Functionalisation with Pyrene-PEG-Rhodamine*. 2022.
- [84] Dusan Vobornik, Maohui Chen, Shan Zou, et al. “Measuring the Diameter of Single-Wall Carbon Nanotubes Using AFM”. In: *Nanomaterials* 13.3 (Feb. 2023), p. 477. ISSN: 20794991. DOI: 10.3390/NANO13030477/S1. URL: <https://www.mdpi.com/2079-4991/13/3/477/htm>%20https://www.mdpi.com/2079-4991/13/3/477.
- [85] David C. Stone. “Application of median filtering to noisy data”. In: 73.10 (Oct. 2011), pp. 1573–1581. ISSN: 0008-4042. DOI: 10.1139/V95-195. URL: <https://cdnsciencepub.com/doi/10.1139/v95-195>.